Journal of Molecular Modeling (2024) 30:240
https://doi.org/10.1007/s00894-024-06026-8

ORIGINAL PAPER

Impact of doping with organic dopants and mixed doping with alkali metals and organic dopants on the absorption, electronic, optoelectronic, thermodynamic and nonlinear optical properties of dibenzo[b,def]chrysene in gaseous media: DFT and TD-DFT studies

C. D. Ribouem A. Bessong[1] · M. T. Ottou Abe[1] · Zounedou Ntieche[1,2] · P. Noudem[1] · J. B. Fankam Fankam[3] · J. M. B. Ndjaka[1]

Received: 17 January 2024 / Accepted: 14 June 2024 / Published online: 2 July 2024

Abstract

Context In this study, we evaluate the geometrical, absorption, optoelectronic, electronic, nonlinear optical (NLO) and thermodynamic properties of dibenzo[b,def]chrysene molecule derivatives by means of DFT and TD-DFT simulations. In view of the aim of producing new high-performance materials for non-linear optics (NLO) by doping test, two types of doping were used. We obtained six derivatives by doping with organic dopants (Nitro, amide and ticyanoethenyl) and mixed alkali metal (potassium) and organic dopants. Doping with organic dopants produced molecules A, B and C, respectively when substituting one hydrogen with nitro (NO_2), amide ($CONH_2$) and tricyanoethenyl (C_5N_3) groups, while mixed doping involved considering A, B and C and then substituting two hydrogens with two potassiums to obtain compounds D, E and F respectively. The negative values of the various interaction energies calculated for all the doped molecules show that they are all stable, but also that molecules C and F are the most stable in the case of both dopings. The gap energies calculated at the B3LYP level of theory are all below 3 eV, which means that all the molecules obtained are semiconductors. Better still, compounds C and F, with gap energies of 1.852 eV and 1.204 eV, respectively, corresponding to decreases of 35.67% and 58.18% in gap energy compared with the pristine molecule, are more reactive than the other doped molecules. Mixed doping is therefore a highly effective way of narrowing the energy gap and boosting the semiconducting character and reactivity of organic materials. Optoelectronic properties have also been improved, with refractive index values higher than those of the reference material, glass. This shows that our compounds could be used under very high electric field conditions of the order of 4.164×10^9 V.m^{-1} for C and 7.410×10^9 V.m^{-1} for F the highest values at the B3LYP level of theory. The maximum first-order hyperpolarizability values for both types of doping are obtained at the CAM-B3LYP level of theory by C: $\beta_{mol} = 92.088\times 10^{-30}$esu and by F: $\beta_{mol} = 129.449\times 10^{-30}$esu, and second-order values are also given by these same compounds. These values are higher than the reference value, which is urea, making our compounds potential candidates for high-performance NLO applications. In dynamic mode and at a frequency of 1064 nm, at the CAM-B3LYP level of theory, the highest dynamic hyperpolarizability coefficients were obtained by C and F. Hyper-Rayleigh scatteringβ_{HRS}, coefficients of the electro-optical Pockel effect (EOPE), EFISHG, third-order NLO-response degree four-wave mixingγ^{DFWM}, quadratic nonlinear refractive index n2 were also calculated. The maximum values of n_2 are obtained by C (6.13×10^{-20} m^2/W) and F (6.60×10^{-20} m^2/W), these values are 2.24 times higher than that of fused silica which is the reference for degenerate four-wave mixing so our molecules could also have applications in optoelectronics as wavelength converters, optical pulse modulators and optical switches.

Methods Using the DFT method, we were able to determine the optimized and stable electronic structures of doped dibenzo[b,def]chrysene derivatives in the gas phase. We limited ourselves to using the proven B3LYP and CAMB3LYP levels of theory for calculating electronic properties, and non-linear optics with the 6-311G + + (d,p) basis set, which is a large basis set frequently used for these types of compound. Gaussian 09 software was used to run our calculations, and Gauss View 6.0.16 was used to visualize the output files. TD-DFT was also used to determine absorption properties at the B3LYP level of theory, using the same basis set.

Extended author information available on the last page of the article

Keywords Dibenzo[b,def]chrysene · Doping · Hyper Rayleigh scattering · Second Harmonic Generation (SHG) · Quadratic nonlinear refractive index

Introduction

Over the last few decades, many researchers have been engaged in the design of new materials with high nonlinear optical response. These have a wide range of applications, including laser technology [1–3], optical data storage [4], ultrafast pulse measurement [5], optical computing [6], high-resolution imaging [7], multiphoton fluorescence [8], optical biodetection [9], optical logic [10].

It has been proven that all systems with excess electrons have an excellent nonlinear optical (NLO) response, which has a direct impact on increasing the value of NLO parameters such as first and second order hyperpolarizability and dipole moment [11]. However, only the value of hyperpolarizability is sufficient to get an idea of the NLO response of any system [9]. Once upon a time, inorganic materials were the only ones known to have NLO properties, but nowadays organic materials with NLO response are gaining ground due to their broad spectrum of actions, which are highly advantageous. These include good transparency, ease of processing and slightly faster response time, high optical susceptibility and lower dielectric constants, by virtue of their laser threshold [3, 12–15].

As a result, scientists are using doping of all kinds to design more and more new organic materials with NLO applications, as these have the major advantage of modifying their physicochemical properties [16]. These modifications can be made by doping certain organic materials with a view to introducing excess electrons and thus increasing the NLO response of these materials. In reviewing the literature on doping, we realize that the dopants used can be of various types. We can have organic dopants (dicyanoethenyl, tricyanoethenyl, amide, hydroxide, nitro, cyano, carboxyl, aldehyde groups), alkali metals, alkaline earth metals, halogens, transition metals, etc., depending on the objectives pursued. We have been inspired by the work of several researchers who have doped organic materials. Noudem et al. in 2022 [17] doped styrylquinoline fragments and obtained the M5 monomer, which is the result of mixed doping (nitro and potassium) of the initial monomer. This work suggests that potassium and nitro doping could be a suitable means of improving the optoelectronic, electronic and NLO properties of styrylquinoline monomer. Fonkem et al. [18] carried out potassium doping of the acrylic acid molecule 2-cyano-3-[4(diphenylamino) phenyl] and the result was a reduction in gap energy, leading to the conclusion that alkali metal doping is an easy way of increasing the conductivity of an organic material. Kenji Tsukamoto et al. [19] doped an organic molecule with the groups dicyanoethenyl and tricyanoethenyl and succeeded in improving its electronic properties. In our previous work [20], we demonstrated the effectiveness of doping the dibenzo[b,def]chrysene molecule with lithium by varying the different doping sites, thus obtaining new molecules with improved NLO response, optoelectronic, electronic and even absorption properties. Other researchers have performed doping using halogens (chlorine, fluorine) [21], alkali metals [22], alkaline earth metals [23] and even transition metals [24]. An increasing number of researchers are carrying out doping tests using other types of dopings to improve the NLO responses of certain materials, such as organic dopants including dicyanoethenyl, tricyanoethenyl, amide, hydroxide, nitro, cyano, carboxyl and aldehyde groups [19, 25–27].

Polycyclic aromatic hydrocarbons (PAHs) are well known for their excellent optoelectronic properties. They are small organic molecules that have been widely used over the last few decades in a number of devices such as photovoltaic cells, light-emitting diodes, liquid crystals and thin-film organic field-effect transistors [19, 28–30]. Polycyclic aromatic hydrocarbons are organic molecules with facilities such as increased non-linear optics, optoelectronics and even optical properties, increased functional groups leading to the modification of certain chemical properties, which is not the case for polymers [31–35]. Dibenzo[b,def]chrysene is one of the PAHs molecules that has been shown to be an organic semiconductor and could provide high power conversion efficiencies in bulk heterojunction solar cells [34–36].

In order to improve the physical and chemical properties of the dibenzo[b,def]chrysene molecule, the search for different dibenzo[b,def]chrysene derivatives has gained momentum in recent times [37]. With this in mind, several researchers have set their sights on this molecule and its derivatives, such as Felix Gagnon et al. [38], who recently studied the photophysical, electrochemical and absorption properties of 2, 9-Dibenzo[b,def]chrysene and found it to be a material of the future with applications in light-emitting diodes, aggregation-induced emission (AIE), field-effect transistors and solar cells. A few years earlier Ying Shu et al. [39] had studied the impact of tetrahedral groups and device processing conditions on the crystal packing, thin film characteristics and OFET hole mobility of 7,14-bis(ethynyl)-dibenzo[b,def] chrysene derived from dibenzo[b,def]chrysene; they came to the conclusion that the compound could have very good semiconducting properties and considerably influence material performance in OFETs. H. Wang et al. [40], studied the vibrational infrared spectroscopy, Raman activity and electronic absorption of neutral Dibenzo[b,def]chrysene and its ionic forms theoretically and experimentally using DFT-B3LYP. F.-J. Zhang, et al. [41] proposed a derivative of the Dibenzo[b,def]chrysene molecule whose electronic, absorbance, photochemical, photophysical and frequency properties were investigated experimentally and theoretically.

In order to achieve our goals, we carried out several different doping with the above-mentioned dopants, while

varying the doping sites with a view to obtaining new materials with a good non-linear response from dibenzo[b,def] chrysene, our initial molecule. So, after all these tests, we opted for doping with organic dopants (nitro, amide and tricyanoethenyl groups), which gave us compounds A, B and C; we continued with mixed alkali metal (K) and organic dopants, which also gave us compounds D, E and F. Our final choice is purely intentional, as our aim is to see the effect of these two types of doping on the behavior of our initial molecule.

Computational methodologies

To determine the optimized electronic structure, vibrational spectra, optoelectronic properties, linear and non-linear optics and thermodynamic properties of gas-phase dibenzo[b,def]chrysene, we used Gaussian 09 [42], a quantum chemistry software package. To carry out our calculations, we used two functionals, B3LYP and CAM-B3LYP, with a 6-311G + + (d,p) basis set. The use of the large basis set such as the 6-311G + + (d,p) has some advantages in reducing the overestimation compared to the smaller basis sets and presents good agreement with experimentals values [43]. Gauss view 6.0.16 [44] was used to visualize our optimized structures. The choice of our two functionals was guided by information contained in the literature [45, 46].

It has been shown that the hybrid B3LYP functional is sufficiently accurate and suitable for calculating the structural, electronic, optoelectronic, charge transfer and thermodynamic properties of organics materials [47–49]. It was also shown that range separated functionals provide better optical rotation prediction than hybrid or pure functionals [50, 51].

As for the CAM-B3LYP functional, it is a long-range corrected hybrid functional that facilitates the net determination of the optical and chemical quantum properties of organic molecules, and also enables a good study of the quantum properties of organic materials. We have used it in our calculations to confirm the predictions of the calculation of nonlinear optical properties [52–54]. Then it was demonstrated to be able to describe accurately charge-transfer transitions in large aromatic molecules [55] for which conventional LDA, GGA, and hybrid functionals perform very poorly [56].

optimized our molecules to make sure they were stable. We then went on to calculate the ground-state properties of our compounds using DFT with the B3LYP and CAM-B3LYP functionals [57], and as a function of time (TD-DFT) using only the B3LYP functional for the first six excited states, while keeping the same 6-311G + + (d,p) basis set. The absorption properties were calculated using TD-B3LYP.

Theoretical background

Here we focus on the calculation of linear and non-linear parameters, which play an undeniable role in the design of new materials with pronounced optoelectronic and non-linear optical (NLO) responses [58, 59]. The dipole moment is a measure of a molecule's polarity. Its expression is given by the equation [60]:

$$\mu = aE + \beta E^2 + \gamma E^3 + \cdots \tag{1}$$

The total value of the dipole moment for any compound is given by:

$$\mu_{tot} = \sqrt{\mu_x^2 + \mu_y^2 + \mu_z^2} \tag{2}$$

The mean value of electrical polarizability [61]:

$$\langle \alpha \rangle = \frac{1}{3}\left(\langle \alpha_{xx} \rangle + \langle \alpha_{yy} \rangle + \langle \alpha_{zz} \rangle\right) \tag{3}$$

The anisotropy [62] of the polarizability can be determined by the components of the polarizability matrix by the equation:

$$\Delta a = \frac{1}{\sqrt{2}}\left[\left(a_{xx} - a_{yy}\right)^2 + \left(a_{yy} - a_{zz}\right)^2 + \left(a_{zz} - a_{xx}\right)^2 + 6\left(a_{xz}^2 + a_{xy}^2 + a_{yz}^2\right)\right]^{\frac{1}{2}} \tag{4}$$

As for MR molar refractivity it is a parameter that is a function of the mean value of polarizability and Avogadro's constant and is given by equation [58]:

$$MR = \frac{4}{3}\pi N_A \langle \alpha \rangle \tag{5}$$

In non-linear optics, first and second order static hyperpolarizability are key parameters for determining the non-linear optical response of an organic material. These quantities are given by the following equations [21, 58]:

$$\beta = \left[\left(\beta_{xxx} + \beta_{xyy} + \beta_{xzz}\right)^2 + \left(\beta_{yyy} + \beta_{yxx} + \beta_{yzz}\right)^2 + \left(\beta_{zzz} + \beta_{zxx} + \beta_{zyy}\right)^2\right]^{1/2} \tag{6}$$

$$\gamma = \frac{1}{5}\left(\gamma_{xxxx} + \gamma_{yyyy} + \gamma_{zzzz} + 2\left(\gamma_{xxyy} + \gamma_{xxzz} + \gamma_{yyzz}\right)\right) \quad (7)$$

where β_{ijk} and γ_{ijkl} are the components of the first and second order hyperpolarizability tensors.

We performed calculations of the NLO properties in frequency-dependent dynamic mode. For this, hyper-Rayleigh scattering [59, 62] was evaluated using the following formula:

$$\beta_{HRS}(-2\omega;\omega;\omega) = \sqrt{\langle\beta_{ZZZ}^2\rangle + \langle\beta_{XZZ}^2\rangle} \quad (8)$$

With $\langle\beta_{ZZZ}^2\rangle$ and $\langle\beta_{XZZ}^2\rangle$ being the orientational averages of the components of the hyperpolarizability tensor β [56, 63] and given by the following equations:

$$\begin{aligned}\langle\beta_{ZZZ}^2\rangle = {} & \frac{1}{7}\sum_{\zeta}^{x,y,z}\beta_{\zeta\zeta\zeta}^2 + \frac{4}{35}\sum_{\zeta\neq\eta}^{x,y,z}\beta_{\zeta\zeta\eta}^2 + \frac{2}{35}\sum_{\zeta\neq\eta}^{x,y,z}\beta_{\zeta\zeta\zeta}\beta_{\zeta\eta\eta} \\ & + \frac{4}{35}\sum_{\zeta\neq\eta}^{x,y,z}\beta_{\eta\zeta\zeta}\beta_{\zeta\zeta\eta} + \frac{4}{35}\sum_{\zeta\neq\eta}^{x,y,z}\beta_{\zeta\zeta\zeta}\beta_{\eta\eta\zeta} \\ & + \frac{1}{35}\sum_{\zeta\neq\eta}^{x,y,z}\beta_{\eta\zeta\zeta}^2 + \frac{4}{105}\sum_{\zeta\neq\eta\neq\xi}^{x,y,z}\beta_{\zeta\zeta\eta}\beta_{\eta\xi\xi} \\ & + \frac{1}{105}\sum_{\zeta\neq\eta\neq\xi}^{x,y,z}\beta_{\eta\zeta\zeta}\beta_{\eta\xi\xi} + \frac{4}{105}\sum_{\zeta\neq\eta\neq\xi}^{x,y,z}\beta_{\zeta\zeta\eta}\beta_{\xi\xi\eta} \\ & + \frac{2}{105}\sum_{\zeta\neq\eta\neq\xi}^{x,y,z}\beta_{\zeta\eta\xi}^2 + \frac{4}{105}\sum_{\zeta\neq\eta\neq\xi}^{x,y,z}\beta_{\zeta\eta\xi}\beta_{\eta\zeta\xi}\end{aligned} \quad (9)$$

$$\begin{aligned}\langle\beta_{XZZ}^2\rangle = {} & \frac{1}{35}\sum_{\zeta}^{x,y,z}\beta_{\zeta\zeta\zeta}^2 + \frac{4}{105}\sum_{\zeta\neq\eta}^{x,y,z}\beta_{\zeta\zeta\zeta}\beta_{\zeta\eta\eta} - \frac{2}{35}\sum_{\zeta\neq\eta}^{x,y,z}\beta_{\zeta\zeta\zeta}\beta_{\eta\eta\zeta} \\ & + \frac{8}{105}\sum_{\zeta\neq\eta}^{x,y,z}\beta_{\zeta\zeta\eta}^2 + \frac{3}{35}\sum_{\zeta\neq\eta}^{x,y,z}\beta_{\zeta\eta\eta}^2 - \frac{2}{35}\sum_{\zeta\neq\eta}^{x,y,z}\beta_{\zeta\zeta\eta}\beta_{\eta\zeta\zeta} \\ & + \frac{1}{35}\sum_{\zeta\neq\eta\neq\xi}^{x,y,z}\beta_{\zeta\eta\eta}\beta_{\zeta\xi\xi} - \frac{2}{105}\sum_{\zeta\neq\eta\neq\xi}^{x,y,z}\beta_{\zeta\zeta\xi}\beta_{\eta\eta\xi} \\ & - \frac{2}{105}\sum_{\zeta\neq\eta\neq\xi}^{x,y,z}\beta_{\zeta\zeta\eta}\beta_{\eta\xi\xi} + \frac{2}{35}\sum_{\zeta\neq\eta\neq\xi}^{x,y,z}\beta_{\zeta\eta\xi}^2 \\ & - \frac{2}{105}\sum_{\zeta\neq\eta\neq\xi}^{x,y,z}\beta_{\zeta\eta\xi}\beta_{\eta\zeta\xi}\end{aligned} \quad (10)$$

The depolarization ratio (DR) [64, 65] of a molecule provides information about its geometry and is given by the equation:

$$DR = \frac{\langle\beta_{ZZZ}^2\rangle}{\langle\beta_{XZZ}^2\rangle} \quad (11)$$

Subsequently we proceeded to determine the third order degenerate four-wave mixture γ^{DFWM} [1] with the aim of going deeper into the investigation of NLO properties. It is given by the following equation:

$$\begin{aligned}\gamma^{DFWM}(\omega) = \gamma^{DFWM}(-\omega;\omega,-\omega,\omega) \approx {} & \frac{1}{3}\gamma(-2\omega;\omega,\omega,0) \\ & + \gamma(-\omega;\omega,0,0) - \frac{1}{3}\gamma\end{aligned} \quad (12)$$

The improved quadratic nonlinear refractive index n_2 [1, 66] was calculated by the following relationship:

$$n_2 = 8.28 \times 10^{-23}\gamma^{DFWM} \quad (13)$$

To enhance our study in the linear and non-linear domain, we evaluated first order susceptibilities in static then in frequency-dependent dynamic mode, second and third order susceptibilities [17, 67, 68], all these properties are given by the following equations:

$$\chi_{ij}^{(1)} = \frac{\alpha_{ij}}{\varepsilon_0 V}; \chi_{ijk}^{(2)}(\omega) = \frac{\beta_{ijk}(\omega)}{2\varepsilon_0 V}; \chi_{ijkl}^{(3)}(\omega) = \frac{\gamma_{ijkl}(\omega)}{6\varepsilon_0 V} \quad (14)$$

Our aim being to explore the NLO parameters of our deep-doped derivatives, we also evaluated the second harmonic generation (SHG) response $\chi^{(2)}(-2\omega, \omega, \omega)$, the linear electro-optic susceptibility $\chi^{\mathrm{LEO}}(\omega)$. Finally we evaluated the third harmonic generation (THG) response $\chi^{(3)}(-2\omega, \omega, \omega, 0)$ and the coefficients related to the dc-Kerr electro-optic effect $\chi^{\mathrm{dc-Kerr}}(\omega)$ and the degenerate four-wave mixing of the third-order NLO response χ^{DFWM}.

All atomic units (au) have been converted to international system and electrostatic units using the following conversion relationships: (α[au] = 1.648778×10^{-41} α[SI] = 0.1482×10^{-24} α[esu], β[au] = 3.206361×10^{-53} β[SI] = 8.639418×10^{-33} β[esu] and γ[au] = 6.235365×10^{-65} γ[SI] = 5.036674×10^{-40} γ[esu]) [69–71].

Results and discussion

Geometrical parameters

The optimized structures of the molecules (A, B, C, D, E, F) shown in Fig. 1 were obtained by doping the initial dibenzo[b,def]chrysene with organic dopants and by mixed doping with organic dopants and alkali metals. Figure 1 shows several atoms: carbon in gray, oxygen in red, nitrogen in blue and potassium in violet. After optimizing our compounds, no negative frequencies were observed, reassuring us of their stability. Using the B3LYP level of theory, we were able to obtain the minimum energy of all our doped molecules. We determined geometrical properties such as interatomic distances and bond angles, which we have summarized in tables s.1 and s.3 for interatomic distances, and tables s.2 and s.4 for bond angles. Overall, we can see that bond lengths have been revised upwards in some cases by doping effects. When we look at the evolution of the value of the C1-C5 bond with doping at the B3LYP level of theory, we see that it is 1.4369 Å for the undoped dibenzo[b,def] chrysene D0 molecule [20], then 1.4368 Å, 1.4369, 1.4371, 1.4366, 1.438 and 1. 4449 Å, respectively for A, B, C, D, E and F, i.e. a slight decrease for compounds A and D which we can explain by the character of the nitro group, this

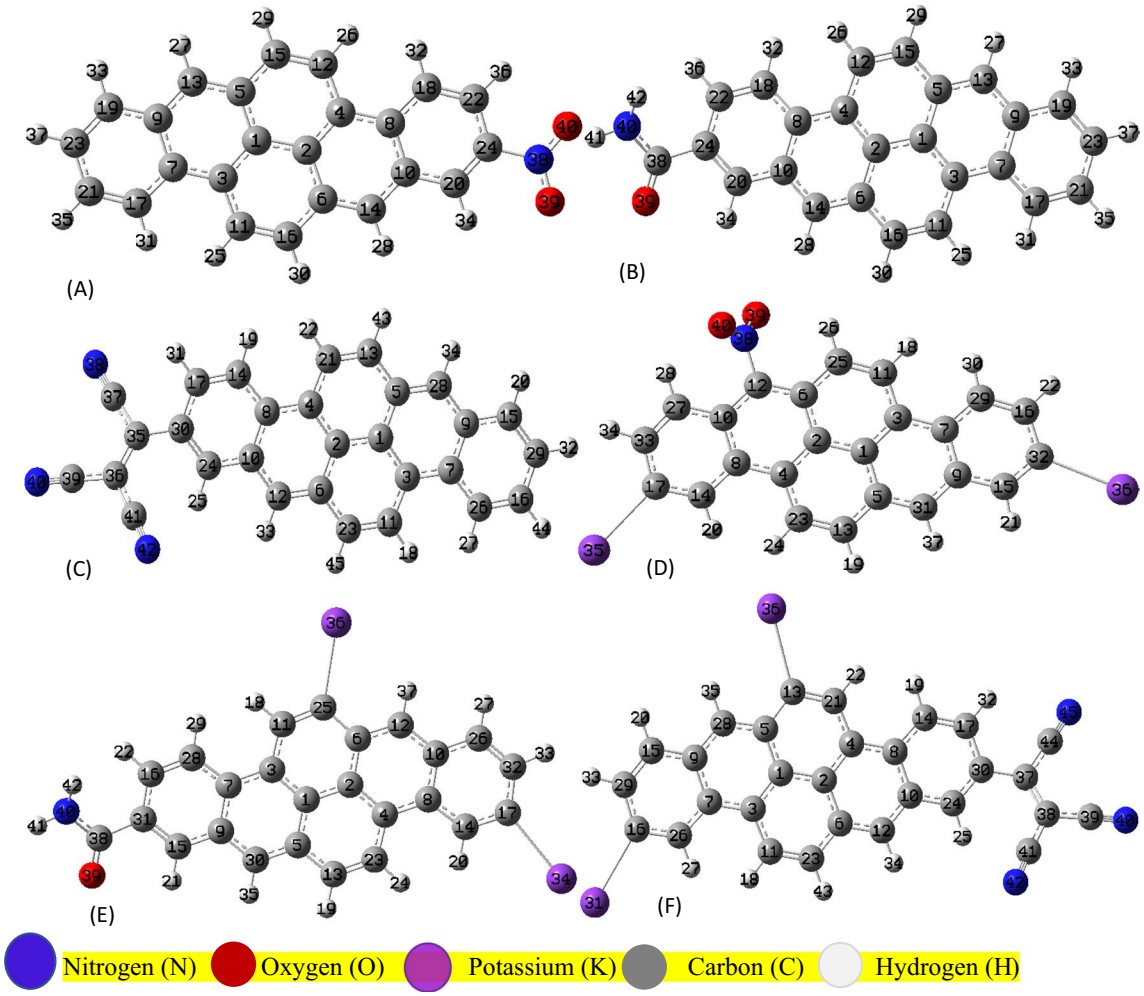

Fig. 1 Optimized structures of our doped dibenzo[b,def] chrysene derivatives at the B3LYP level of the theory with the 6–311 + + G(d,p) basis set. **A**: doped with nitro group; **B**: doped with amid group; **C**: doped with tricyanoethenyl group; **D**: doped with two potassiums and nitro group; **E**: doped with two potassiums and amid group; **F**: doped with two potassiums and tricyanoethenyl group

value remains constant when replacing the hydrogen with the amide group (B), and increases by 0.014%, 0.076% and 0.56% respectively when doped with the tricyanoethenyl group (C), the amide group and two potassiums (E) and the tricyanoethenyl group and two potassiums (F). In terms of the C-H bond of our doped molecules, we make the same observation, obtaining maximum values of 1.0854 Å, 1.0855 and 1.0854 Å when doped with nitro, amide and tricyanoethenyl respectively, and 1.0945 Å, 1.0904 and 1.0904 Å when mixed doping with nitro, amide and tricyanoethenyl plus two potassiums at the B3LYP level of theory. We have an increase of 0.0091 Å, 0.0049 and 0.005 Å depending on whether we go from A to D, B to E and C to F, enabling us here to evaluate the effects of the substitution of the two potassium atoms, which are electron donors, on the C-H distances [40]. We can thus affirm that there is a good correlation between our results and those of dibenzo[b,def]chrysene contained in the literature.

With regard to the C = C bond lengths we obtained, we note that the average value is approximately equal to 1.37 Å for all molecules, with the exception of compound C for which the C24 = C30 distance is equal to 1.3842 Å at the B3LYP level of theory. Our C = C values are quite close to 1.34 Å for ethylene obtained by A. Veillard [72]. We believe that, due to the pi and sigma conjunction of the C = C double bond, which is a conjugated bond, the effects of doping are less perceptible, since axial overlap here is not possible as in the case of C–C, but rather lateral. This observation can also be seen in the values obtained with CAM-B3LYP, which show that the double bond can vary very little due to the doping effect of dibenzo[b,def]chrysene.

The highest values of potassium carbon bond lengths (C-K) obtained for D, E and F are 2.6664 Å, 2.6664 Å and 2.6722 Å respectively, and we note that the distance (C-K) remains constant for D and E increases by 0.217% compared with D and E for F. We believe this difference may be due to the presence of

three cyano groups, which are strongly attractive groups due to the presence of the carbon–nitrogen triple bond.

In compounds B and E, which are obtained by doping with the amide group and by doping with the amide group plus two potassium groups respectively, the C = O interatomic distance varies from 1.2259 Å for B and 1.2279 Å for E at the B3LYP level of theory, i.e. an increase in this distance of 0.163% due to the presence of two potassiums as donors.

The C-N single bond is also present in compounds A, B, D and E, due to the presence of nitro (NO2) and amide (CONH2) groups. The length of this bond varies according to the group involved, so we have 1.4756 Å, 1.502 Å, 1.4748 Å and 1.3784 Å with A, B, D and E respectively. For E, this distance decreases by 8.23% when two hydrogens are substituted by two potassiums, and remains virtually constant. We can nevertheless report a decrease in the C-N distance by substitution with potassiums. We suggest that this may be due to the strong electronegative character of nitrogen in front of potassium. On the other hand, we have the C≡N triple bond of compounds C and F, whose bond lengths are 1.1558 Å and 1.1567 Å respectively, with a slight increase due to substitution of hydrogens by potassiums. Finally, we have the N–H bonds, whose bond length remains constant at 1.0088 Å for B and E, and N = O, whose bond lengths vary very little, i.e. 1.2259 Å for A and 1.2279 Å for D.

The tables s.2 and s.4 contained in the supplementary materials, group together all values of the bond angles between the different atoms of our six doped molecules. We can already see that these angles increase with doping regardless of the method used. We also note that the highest value of bond angles in the case of doping with organic dopants is given by C i.e. (C30,C35,C36) = 127.0855° and the lowest value is (C39,C36,C41) = 114.7375° also given by C, at the B3LYP level of theory, while the largest value in the case of mixed doping is given by E i.e. (C32,C17,K34) = 148.5232° and the smallest value is also given by E i.e. (C14,C17,K34) = 97.068° at the CAM-B3LYP level of theory. The H. Wang's work [40] on dibenzo[b,def]chrysene revealed that the values of the of the C–C-C and C–C-H angles are close to 120°, with slight deviations of 5°. In line with this work, we can say that our results are valid, as the average values of these angles for our doped molecules oscillate around 119° and 121°, with exceptions made for angles close to the doping zones, such as (C32,C17,K34) = 148.5232° with CAM-B3LYP and (C32,C17,K34) = 134.4063° with B3LYP, which sometimes show an increase of almost 28° and 14° at these respective levels of theory. Our observations show that bond angle values increase with doping, i.e. the substitution of hydrogens by potassium. This could be explained by the fact that, in order to reach the energy minimum, the new molecules must undergo modifications to their geometric structure, which have a direct impact on bond lengths and angles, electronic, optical, optoelectronic and even reactivity properties, due to the delocalization of electrons in the system. As a result, our new doped molecules can have a much larger field of application than the undoped molecule.

Vibrational spectroscopy analysis

Raman and infrared (IR) spectroscopies are used to measure vibrational frequencies and molecular phonons. These techniques have a proven track record in determining the structure and chemical composition of molecules [73, 74]. The combined analysis of the two spectra of a compound provides a wealth of information on its composition and structure, which is not the case when only one of the techniques is used [75]. In this section, we have used the B3LYP and CAM-B3LYP levels of theory to carry out the vibrational analysis of our six doped molecules A, B, C, D, E and F. Molecules A and D, B and E, C and F each have 40, 42 and 45 atoms respectively, implying that these molecules have 114, 120 and 129 normal modes of vibration active in Infrared (IR) absorption and Raman scattering respectively. No negative frequencies were obtained, proving that all minima obtained at the surface potential energy of our compounds are local minima. Tables S.5 – S.10 in the supplementary materials summarize selected frequency values, and Figs. 2, 3, 4 and 5 show the IR and Raman spectra of our compounds. Vibrations between two atoms, still called stretches, are represented by the letters r and R, in-plane bending vibrations are materialized by the letters α and β, and finally out-of-plane vibration modes are indicated by the letters ϵ and τ. In addition to the experimental assignments made by H. Wang et al. [40], we also used the Gauss view software [44] to suggest assignments related to the dopants used, which obviously have a remarkable influence on our spectra and compared to literature results.

In general, C-H stretching vibrations in aromatic compounds oscillate between 3000 and 3200 cm^{-1} [76, 77]. This range is sometimes strongly influenced by the nature of the substituents. In our study, the normal modes calculated in the ranges 3159.32—3229.13 cm^{-1}, 3030.94—3214.14 cm^{-1}, 3157.57—3213.93 cm^{-1}, 3068.82—3203.40 cm^{-1}, 3161.19—3218.61 cm^{-1} and 3076.85—3211.67 cm^{-1} can be assimilated to asymmetric and symmetric C-H stretching modes for A, D, B, E, C and F respectively at the B3LYP level of theory. According to experimental studies carried out by H. Wang et al. [40] on our pristine molecule, these vibrations are perceived in the region 2861.5 – 2966.1 cm^{-1}, i.e. a difference oscillating between 169.44—263.03 cm^{-1}. This discrepancy between the experimental data can be explained by the conditions taken into account during the experiment, and also by the fact that doping brings an excess

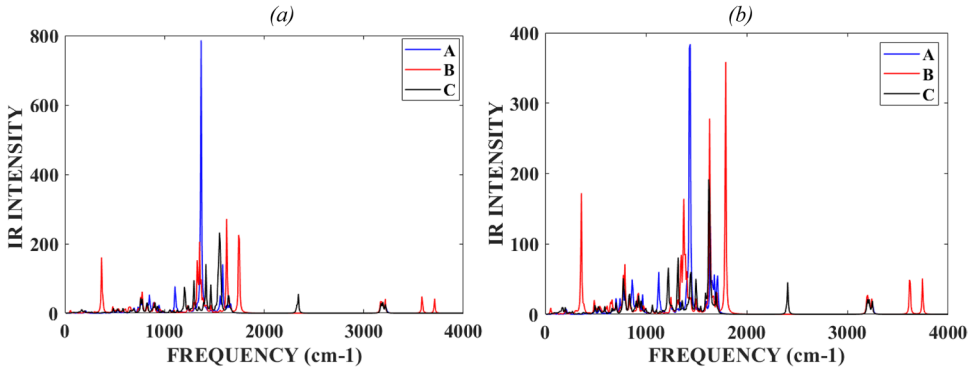

Fig. 2 IR intensity (**a**) (organic doping at B3LYP level) and IR intensity (**b**) (organic doping at CAM-B3LYP level)

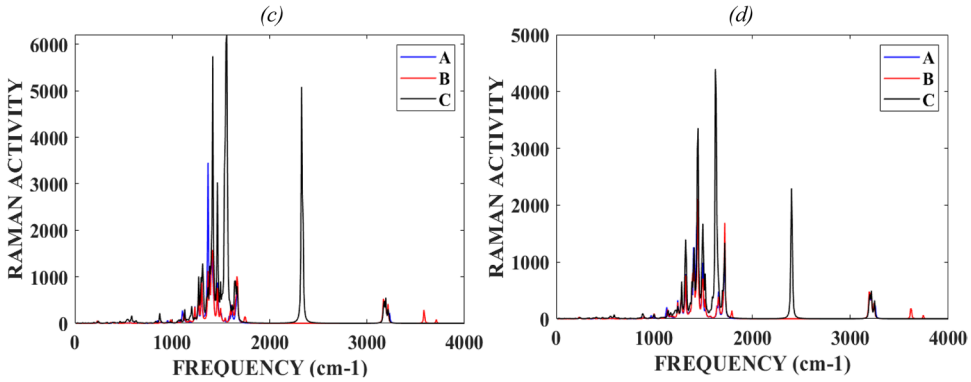

Fig. 3 Raman Activity (**c**) (organic doping at B3LYP level) and Raman Activity (**d**) (organic doping at CAM-B3LYP level)

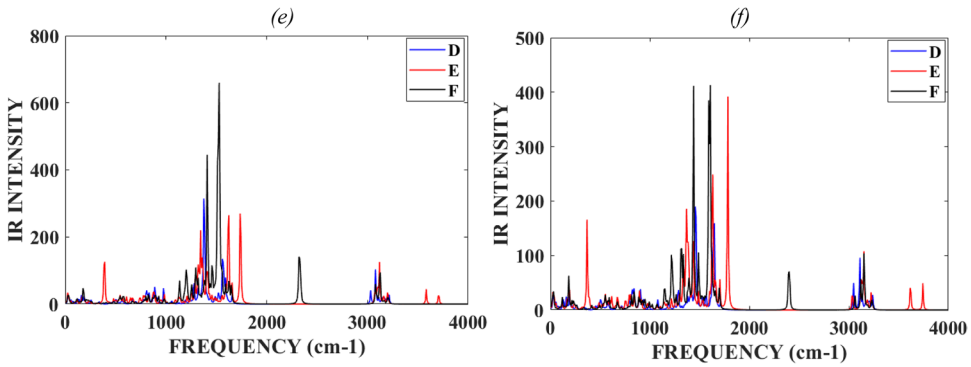

Fig. 4 IR intensity (**e**) (mix doping alkali metals and organic doping at B3lyp level) and IR intensity (**f**) (mix doping alkali metals and organic doping at CAM-B3LYP level)

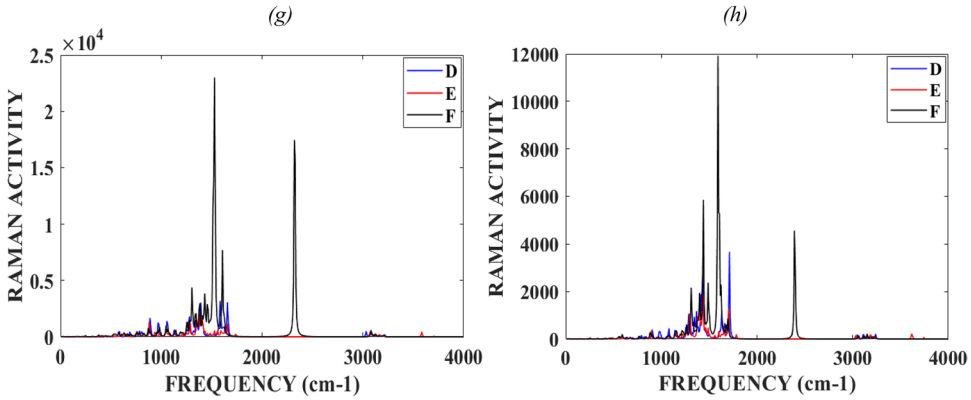

Fig. 5 Raman Activity (**g**) (mix doping alkali metals and organic doping at B3lyp level) and Raman Activity (**h**) (mix doping alkali metals and organic doping at CAM-B3LYP level)

of electrons which increases the reactivity of doped structures and many other parameters. However, the values we obtained are fairly close to those found in the literature [40, 78].

In the infrared absorption and Raman scattering spectra of A, D, B, E, C and F, we observe a set of peaks contained in the areas 1398.77 -1664.70 cm^{-1}, 1386.37—1653.60 cm^{-1}, 1397.48—1663.97 cm^{-1}, 1390.55—1650.60 cm^{-1}, 1359.93—1664.07 cm^{-1} and 1356.29—1645.47 cm^{-1} at the B3LYP level of theory, which we attribute to C = C conjugate vibration modes. According to the literature, this interval lies between 1430 and 1625 cm^{-1} [79, 80]. On the other hand, C–C vibration modes are very often found in the 1200—1650 cm^{-1} range [81].

For our molecules, we perceive C–C stretching vibrations in the regions 1228.09 -1664.70 cm^{-1}, 1205.07—1653.60 cm^{-1}, 1225.14—1663.97 cm^{-1}, 1203.85—1650.60 cm^{-1}, 1226.49—1664.07 cm^{-1} and 1197.39—1645.47 cm^{-1} at the B3LYP level of theory. When compared with the results obtained for D0 [20], there is a slight difference between these ranges obtained for the C = C and C–C vibration modes. However, the discrepancy observed between the experimental data and our theoretical values may be due to the effects of the doping carried out.

In the absence of experimental data, we were unable to assign all the vibrational modes exhibited by our doped molecules. Nevertheless, using Gauss view software [44] we suggest that vibrations occurring at frequencies 179.55 and 212.01 cm^{-1}, 156.91 and 172.03 cm^{-1}, 115.54 and 130.88 cm^{-1} respectively for D, E and F at the B3LYP level of theory could be assigned to C-K vibrational stretches. As for the C-N vibrational stretches, we obtained them in the ranges of 1357.56—1361.69 cm^{-1}, 1369.21—1375.12 cm^{-1}, 1346.37—1361.73 cm^{-1} and 1306.72—1357.28 cm^{-1} with B3LYP for molecules A, D, B and E respectively. The C = O stretching frequencies obtained at B3LYP theory level for our B and E molecules are 1743.32 cm^{-1} and 1734.79 cm^{-1} respectively. Within compounds C and F, we also have frequencies obtained in the ranges 2319.54—2339.62 cm^{-1} and 2309.44—2334.05 cm^{-1} corresponding to C≡N vibrational stretches. Compounds B and E then show N–H vibrational stretching at frequencies 3585.65 cm^{-1} and 3710.30 cm^{-1} for B, followed by 3583.24 cm^{-1} and 3707.13 cm^{-1} for B3LYP. Finally, we have the N = O stretches that appear in compounds A and D in the intervals 1553.51—1602.63 cm^{-1} for A and 1555.41—1580.43 cm^{-1} for D at the B3LYP level of theory [82, 83].

Optoelectronic properties

We have performed DFT calculations in order to determine optoelectronic properties such as: volume (V), average electric field (E), polarization density (P), electric susceptibility (χ), dielectric constant (ε), refractive index (n), and electric displacement (D) of doped dibenzo[b,def]chrysene derivatives. All values of these quantities are reported in Table 1. The dipole moment is due to the fact that the barycenter of negative charges coincides with the barycenter of positive charges, otherwise the molecule is said to be apolar with a zero-dipole moment; it can also be caused by the application of an external electric field. The dipole moment is linked to the electric field by the relation $\mu = \alpha E + \beta E^2 + \gamma E^3 + \ldots$. So we have the formulas giving the electric field and polarization density given by the equations $E = \frac{\mu}{\alpha}$ and $P = \frac{\mu}{V}$. For the other quantities mentioned above, we have used formulas taken from the literature [70, 84, 85]. In view of the values obtained and summarized in Table 1, we can see that all the calculated parameters have virtually increased with the various doping operations carried out. However, by comparison with the calculations performed on our initial centrally symmetrical molecule, we can say that doping significantly improved the optoelectronic behavior of our material. As regards the electric field, polarization density, electric susceptibility and electric displacement, all linearly related and proportional to the dipole moment, for the initial molecule all these values were zero, but with doping we

Table 1 Volume V, electric field E, density polarization P, electric susceptibility χ, dielectric constant ε, refractive index n, magnitude of the displacement vector D of dibenzo[b,def]chrysene derivatives (A, B, C, D, E and F), obtained at the CAM-B3LYP and B3LYP levels of theory with 6–311 + + G(d,p) basis set

Methods	B3LYP						CAM-B3LYP					
Molecules /properties	A	B	C	D	E	F	A	B	C	D	E	F
$V \times 10^{-28}(m^3)$	1.691	1.655	2.002	1.765	2.337	2.810	1.583	1.794	2.225	1.646	1.813	2.914
$E \times 10^9(V.m^{-1})$	3.855	2.081	4.164	6.461	5.729	7.410	3.918	2.204	4.164	7.729	5.580	7.630
P ($C.m^{-2}$)	0.140	0.078	0.164	0.300	0.201	0.276	0.142	0.072	0.134	0.335	0.220	0.229
χ	4.102	4.233	4.448	5.244	3.962	4.207	4.093	3.690	3.635	4.895	4.453	3.390
$\varepsilon(10^{-11}\,C.V^{-1}\,m^{-1})$	4.517	4.633	4.824	5.528	4.393	4.610	4.510	4.152	4.104	5.220	4.828	3.887
n	2.258	2.287	2.334	2.499	2.228	2.282	2.257	2.166	2.153	2.428	2.335	2.095
$D(C.m^{-2})$	0.174	0.096	0.201	0.357	0.252	0.342	0.177	0.092	0.171	0.403	0.269	0.297

obtain for these quantities respectively E = 7.630 × $10^9 V.m^{-1}$ for F, P = 0.335 C.m^{-2} for D, χ=5.244 for D and D = 0.403 C.m^{-2} for D. These values obtained would be due to an increase in charge carriers with the addition of the amide and tricyanoethenyl groups and the two potassiums, which are electron donors. We also note that mixed doping with organic dopants plus alkali metals has a better optoelectronic response than simple doping with organic dopants alone.

The values of the electric field E of our different molecules decrease according to 7.410 > 6.461 > 5.729 > 4.164 > 3.855 > 2.081 × $10^9 V.m^{-1}$ respectively for molecules F, D, E, C, A and B at the B3LYP level of theory; and 7.729 > 7.630 > 5.580 > 4.164 > 3.918 > 2.204 × $10^9 V.m^{-1}$ respectively for molecules D, F, E, C, A, B at the CAM-B3LYP level of theory. From this observation we can say that the CAM-B3LYP level of theory is the one that gives us the highest electric field values and the mixed nitro plus two potassium doping is the one for which charge carrier activity is the most intense in view of its high electric field value. By comparing the electric field values obtained in the case of lithium doping of the pristine molecule [20], for which the field value given by D1 (4.720×$10^9 V.m^{-1}$) with the B3LYP functional, we can only confirm that mixed alkaline and organic doping leads to higher field values and therefore offers us a wider field of application in optoelectronics. For polarization density and electric displacement, we have almost the same behavior as for the electric field, except that in both cases compound D has the highest values, regardless of the method used. Taking the case of polarization density, we note in comparison with the initial dibenzo[b,def]chrysene D0 [20] that doping resulted in an improvement of 0.30; 0.276; 0.201;0.164; 0.140; 0.078 C.m^{-2} respectively for D, F, E, C, A and B with the B3LYP functional. Comparing these values with those obtained in our previous work on lithium doping, we realize that mixed alkali metal and organic doping gives the best results for optoelectronics. The electrical displacement values obtained decrease to 0.357; 0.342; 0.252; 0.201; 0.174; 0.096 C.m^{-2} respectively for D, F, E, C, A and B at the B3LYP level of theory. This finding could be explained by the fact that doping has impacted charge distribution, causing a drastic decrease in dipole moment and thus reducing optoelectronic property values. Based on the work of Mveme et al. [60], we can say that the high P and D values of D, E and F molecules could also be potential pyroelectric and piezoelectric materials.

Refractive index, electrical susceptibility and dielectric constant are related quantities, so when χ increases, ε increases and consequently n increases too. With compound D, we obtained the highest values ($\chi = 5.244, \varepsilon = 5.528\times10^{-11}$ C.V^{-1} m^{-1} et n = 2.499) of the six molecules studied according to Table 1 with the B3LYP level of theory. The high values of electrical susceptibility and dielectric constant of our compound show that it is the one whose electron cloud could deform more rapidly if subjected to an external electric field, and where we would have easy electron delocalization compared to the other compounds. On this basis too, it is positioned as the compound with the best optoelectronic behavior compared with the others. The refractive index is a parameter characterizing the interaction between light and matter, and depends on the characteristics of the medium and the incident electromagnetic wave. The value of the refractive index increases with doping, regardless of the method used, compared with the initial dibenzo[b,def]chrysene: with the B3LYP method we obtained n(E) = 2.228, n(A) = 2.258, n(F) = 2.282, n(B) = 2.287, n(C) = 2.334 and n(D) = 2.499, i.e. an increase in refractive index of the order of 122. 8%, 125.8%, 128.2%, 128.7%, 133.4% and 149.9% respectively when doping our initial molecule with the amide group and two potassiums, the nitro group, the tricyanoethenyl group and two potassiums, the amide group, the trycyanoethenyl group, the nitro group and two potassiums. By comparing our refractive index values with those of glass [86] (n = 1.5), we can say that the surplus of electrons provided by the doping makes the doped derivatives increasingly less transparent and opposes the propagation of electromagnetic waves through them.

Electronic properties and global reactivity descriptors

In order to discuss the semiconducting character, stability and even reactivity of our molecules obtained by doping dibenzo[b,def]chrysene, we have calculated the electronic properties and global reactivity descriptors at the B3LYP and CAM-B3LYP levels of theory using the 6–311 + + G(d,p) basis set, the values of which are reported in Table 2.

In terms of electronic properties, the LUMO energy is the lowest energy assigned to the unoccupied molecular orbital. When this value is high, the compound yields electrons. In the case of our compounds, the value of this quantity follows this ascending order $C < F < A < B < D < E$ whatever method used. This implies that mixed doping (2 K + amide) results in a compound (E) that is more electron-donating than the others. The LUMO energy values of compounds E and D at the B3LYP level of the theory are close to that of the BSA-3 molecule, derived from triphenylamine-carbazole, whose LUMO energy value is 1.96 eV [87].

The HOMO energy is the energy of the most occupied molecular orbital, and it also tells us something about the donor and acceptor character of our compound. Compared with the values obtained in this work, the HOMO energy values decrease in the following order: -3.964 eV, -4.248, -4.393, -5.380, -5.653 and -5.794 eV respectively given by

Table 2 E_{HOMO}, E_{LUMO}, gap energy (Egap), chemical potential μ_{CP}, hardness η, ionization potential IP, electronic affinity EA, electronegativity χ, softness S, electrophilicity index ω, nucleophilicity index ν and maximum charge transfer ΔNmax of dibenzo[b,def]chrysene derivatives (A, B, C, D, E and F), obtained at the CAM-B3LYP and B3LYP levels of theory with 6–311 + + G(d,p) basis set

Methods	B3LYP						CAM-B3LYP					
Molecules /properties	A	B	C	D	E	F	A	B	C	D	E	F
E_{HOMO} (eV)	-5.653	-5.380	-5.794	-4.248	-3.964	-4.393	-6.750	-6.485	-6.862	-5.320	-5.052	-5.397
E_{LUMO}(eV)	-2.984	-2.523	-3.942	-1.697	-1.597	-3.187	-1.842	-1.460	-2.812	-0.975	-0.863	-2.145
E_{Gap}(eV)	2.668	2.856	1.852	2.551	2.367	1.204	4.907	5.025	4.050	4.344	4.190	3.252
μ_{CP}(eV)	-4.319	-3.951	-4.868	-2.973	-2.781	-3.79	-4.296	-3.973	-4.837	-3.147	-2.957	-3.771
η(eV)	1.334	1.428	0.926	1.276	1.184	0.603	2.454	2.513	2.025	2.173	2.095	1.626
IP(eV)	5.653	5.380	5.794	4.248	3.964	4.393	6.750	6.485	6.862	5.320	5.052	5.397
EA(eV)	2.984	2.523	3.942	1.697	1.597	3.187	1.842	1.460	2.812	0.975	0.863	2.145
χ(eV)	4.319	3.951	4.868	2.973	2.781	3.79	4.296	3.973	4.837	3.147	2.957	3.771
S(eV^{-1})	0.750	0.700	1.080	0.784	0.845	1.658	0.407	0.398	0.494	0.460	0.477	0.615
ω(eV)	6.997	5.466	12.796	3.463	3.266	11.911	3.760	3.141	5.777	2.279	2.087	4.373
ν(eV^{-1})	0.143	0.183	0.078	0.289	0.306	0.084	0.266	0.318	0.173	0.439	0.479	0.229
ΔN_{max}	3.238	2.767	5.257	2.330	2.349	6.285	1.751	1.581	2.389	1.448	1.411	2.319

E, D, F, B, A and C at the B3LYP level of theory. This result confirms once again that compound E is very easy to transfer electrons. This is also justified by the nature of the doping used, as we can see that mixed doping makes molecules easy to transfer electrons. The same behavior is observed with CAM-B3LYP level of theory. At the B3LYP level of the theory, the HOMO energy of compounds D, E and F are close to those of the BSA molecule and its derivatives. This leads us to conclude that our mixed-doping molecules are very good acceptors and could have the same electronic and NLO applications as the latter [87].

Gab energy is a key parameter that provides information on the conductivity of organic materials, as well as on the reactivity and stability of molecular systems. When the gab energy value is low, i.e. the bandgap width is very small, the molecule is less stable, less rigid, more reactive, more chemically polarizable and the transition of electrons from the conduction band to the valence band is rapid. On the other hand, when the bandgap width is larger, the material is more chemically stable, less reactive and more rigid [21, 31, 88]. At the B3LYP level of theory, all the gap values obtained are below 3 eV, which means that these compounds all have good semiconducting properties. Thus we obtained Eg = 2.856 eV for compound B, a value roughly equal to that obtained for D0 the initial molecule 2.879 eV [20]. This shows that the substitution of the hydrogen by the amide group has no considerable effect on the conductivity of our material. This energy gap is reduced slightly by the substitution of a nitro group (compound A), bringing the value up to 2.668 eV, i.e. an increase in conductivity of 7.32% compared with the initial value. With the substitution of a hydrogen by the tricyanoethenyl group (compound C), the gap value was lowered by 1.027 eV, representing a percentage reduction of 35.67%, enabling us to conclude that doping with organic dopants is a means of improving the semiconducting properties of organic materials. We continued our work with mixed doping as described above, obtaining values of 2.551 eV, 2.367 eV and 1.204 eV for D, E and F respectively, i.e. a reduction of 0.328, 0.512 and 1.675 eV. With compound F, we were able to lower the gap energy by more than fifty percent, or 58.18%. Comparing the gap value of F with that obtained with D4 [20] in our previous article, we find a difference of 0.497 eV, which means that compound F is more reactive than D4, and all the potential applications of D4 are the same for F. A further comparison of these energy gap values of our doped molecules with the energy gap values obtained by M. Usman Khan et al. [87] for the BSA molecule and its derivatives reveals a very interesting similarity between our values, more precisely for the compounds BSA-2 (1.97 eV), BSA-7 (1.53 eV) and BSA-9 (1.49 eV), which are quite close to those obtained for our C (1.852 eV) and F (1.204 eV) molecules. This segment also illustrates that by incorporating different electronegative acceptor groups in the proposed molecules, we would substantially reduce the NLO response and, consequently, the band gap values. With the CAM-B3LYP level of theory, all the gap values obtained are greater than 4 eV except for F, which gives a gap of 3.252 eV, meaning that it is still semiconducting and the others are all insulating. These gab energy values obtained for our molecules A, B, C, D and E at the CAM-B3LYP level of theory, are very close to those obtained for the compound SLN and its derivatives doped at the CAM-B3LYP level of theory also with a different 6-31G(d,p) basis set by M.U. Khan et al. [89]. In view of this similarity of energy gap values, we can confirm that our doped molecules obtained in this work are all potential

canditates for electronics applications with very high nonlinear optics response. Figure 6 and figure s.1 in the supplementary material presents the HOMO and LUMO molecular orbital of our six doped molecules studied respectively at B3LYP and CAM-B3LYP, in order to determine the charge transfer process in our compounds. The areas where the acceptance of electrophiles is most favorable is represented by the red color, and the areas where nucleophiles are more favorable are represented by green color. Of all our doped molecules, it's B derivative that has difficulty transferring electrons from HOMO to LUMO in terms of its diagram, due to the high value of its gab energy. We say that compounds C and F are the most reactive and are the least stable than the others in view of their lower gab energies than the other compounds A, B, D and E. We suggest, in terms of potential applications, that F and C could be used as materials for solar cells and the others could be used for the design of display devices.

We continued by examining on the basis of the optimization of dibenzo[b,def]chrysene doped derivatives in the gas phase, global reactivity descriptors such as ionization potential (IP), electron affinity (AE), electronegativity (χ), chemical hardness (η), chemical softness (S), chemical potential (μ), electrophilicity index (ω), nucleophilicity index (υ) and maximum charge transfer (ΔNmax). The formulas used to calculate the values of these parameters can be found in the

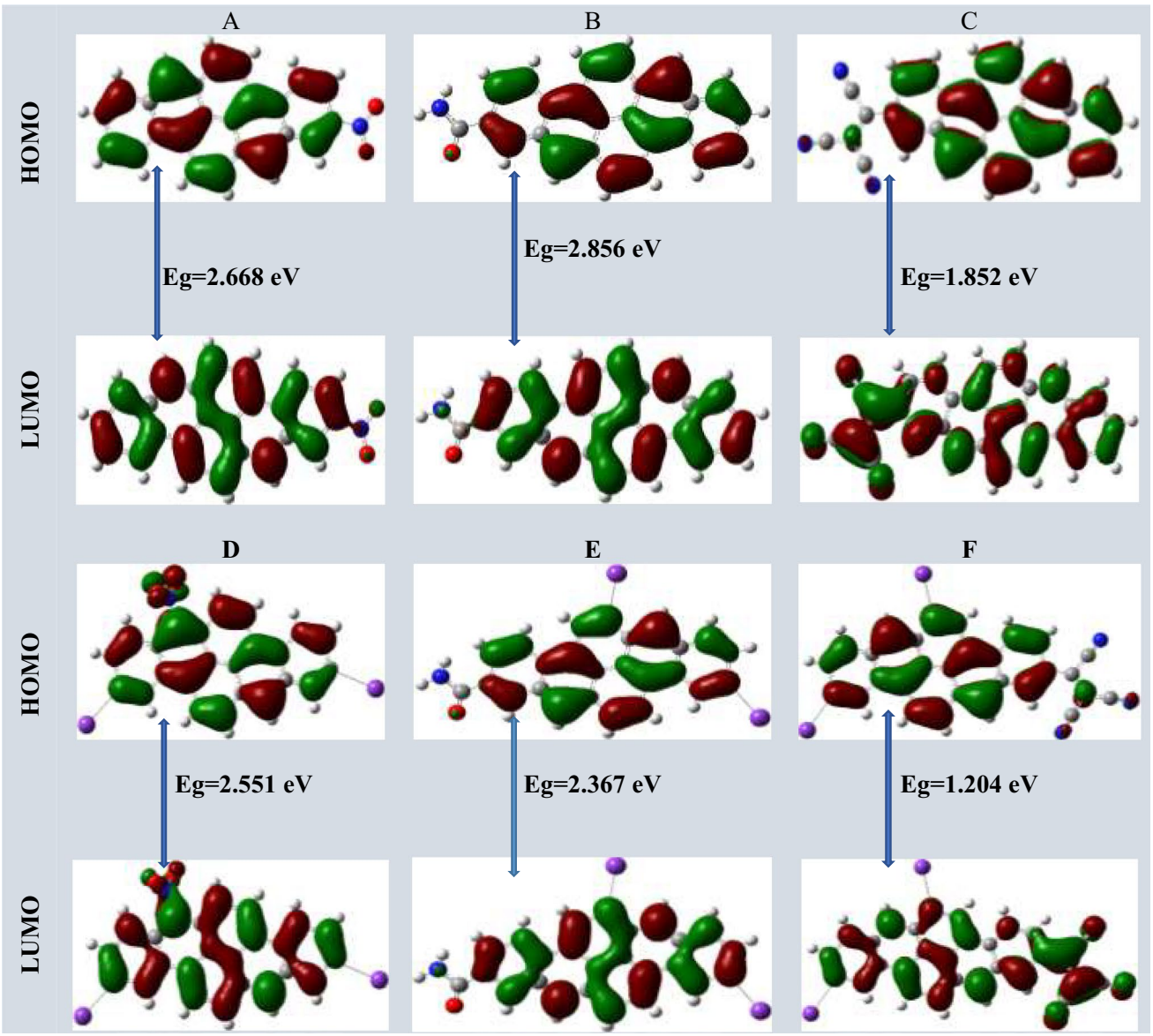

Fig. 6 HOMO and LUMO molecular orbitals of the doped derivatives (**A**, **B**, **C**, **D**, **E** and **F**) of dibenzo[b, def]chrysene obtained at the B3LYP level of theory with the 6–311 + + G(d,p) basis set

literature [51, 81] and are summarized in Table 2 All these values are obtained on the basis of HOMO–LUMO energies and allow us to discuss the chemical stability of our compounds at both the B3LYP and CAM-B3LYP levels of theory.

The ionization potential (IP) is the amount of energy required to eject an electron from a molecule. When the ionization energy is low, the molecule is more reactive, whereas a high ionization energy suggests high system stability, i.e. limited chemical activity. Our calculations gave us the following IP values 5.653 eV, 5.380 and 5.794 eV respectively when replacing hydrogen by a nitro, amide and tricyanoethenyl group at the B3LYP level of theory. We note that these three values are higher than that of the initial compound DO 5.241 eV [20], implying that slightly more energy is required to extract an electron from A, B and C than is required for D0. With the addition of two potassiums to compounds A, B and C we obtain compounds D, E and F whose IP values 4.248, 3.964, 4.393 eV respectively are lower than that of D0. We note a reduction in IP of 18.94%, 24.36% and 16.18%, which means that the addition of alkali metals is an adequate means of reducing the ionization energy of our pure molecule. We observe a similar behavior of IP evolution with the CAM-B3LYP level of theory, except that in this case all IP values are higher than those of the initial D0 molecule, which means that at this level of theory, the doped derivatives are more stable and less reactive than dibenzo[b,def]chrysene D0.

Electron affinity (AE) is the amount of energy released when an electron is added to a neutral molecule; it provides information on a molecule's tendency to always retain its electrons. The calculated values of this quantity (AE) evolve in much the same way as those of the ionization potential at the two levels of theory used, in ascending order of E $< D < B < A < F < C$. The largest value of (AE) 3.942 eV is given by C for doping with the tricyanoethenyl group followed by 3.187 eV for mixed doping (tricyanoethenyl and 2 K) compound F all at the B3LYP level of theory. By comparison with the values of the initial molecule D0 and D1 doped with lithium [20], we find that the electron affinity of compounds C and F undergo an increase of 66.96% and 35% respectively compared with D0, and more than twice that of D1. Thus, mixed and organic doping is one possible way of increasing the electronic affinity of an organic molecule.

Negative chemical potential values (μ_{CP}) provide information on the stability of the molecule or its difficulty in decomposing into its own elements [17]. The chemical potential decreases as follows at the B3LYP level of theory: -3.951, -4.319 and -4.868 eV respectively for molecules B, A and C for doping with organic dopants, -2.781, -2.973 and -3.79 eV respectively for compounds E, D and F for mixed doping. The same trend is observed at the CAM-B3LYP level of theory. These chemical potential values obtained in the case of both doping types imply that compounds C and F are the most reactive they have the smallest chemical potential values among all other compounds.

Chemical hardness (η) is a quantity that characterizes the resistance of the molecule's electron cloud to deformation when subjected to slight perturbations. Thus, if the bandgap width is high, the molecule will be hard, weakly polarizable, with very low chemical and biological activity and high kinetic sensitivity, whereas when the bandgap width is small, the molecule is soft, easily polarizable, with very high chemical and biological activity but low kinetic sensitivity [90]. With both B3LYP and CAM-B3LYP, the smallest values of chemical hardness are those given by compound F whatever the type of doping, i.e. a value of 0.603 eV with B3LYP and 1.626 eV with CAM-B3LYP. This shows that B3LYP is the method that best enables us to appreciate the hardness of our system. Compared with the value obtained for the initial molecule [20], B3LYP reduces the hardness of our molecule by 56.25%. Thus, with doping, the molecule starts to release more and more electrons in its vicinity, which justifies the fact that the initial compound D0 is more stable than F, while compound F is more conductive than D0, hence its good semiconducting character compared with the other molecules. As for chemical flexibility (S), this is a parameter whose variation follows the opposite path to that of chemical hardness (η), whatever the method used and the type of doping performed. The highest value $S = 1.658\ eV^{-1}$ given by F and the lowest value $S = 0.694\ eV^{-1}$ given by D0 [20], effectively confirm this. As far as electronegativity is concerned, we found that it decreases when two potassiums are added to compounds A, B and C, giving rise to mixed doping. It is higher for organic doping, with the highest $\chi = 4.868$ eV value given by compound C with B3LYP. This value reduces with mixed doping, where the highest value is given by F, i.e. $\chi = 3.79$ eV. At CAM-B3LYP theory level, compounds C and F also have the highest values, at 4.837 and 3.771 eV respectively. So, we can say that these molecules are good electron acceptors.

The global electrophilicity index (ω) measures the stabilization energy of a molecule following an external electron charge or its resistance to electron exchange with the system [58]. We note that the values obtained for this magnitude at the B3LYP level of theory, increase as electrons are added to the system by 5.466, 6.997, and 12.796 eV for B, C and C respectively in the case of doping with organic dopants. When two potassiums are added, we obtain 3.266, 3.463 and 11.911 eV for E, D and F respectively, i.e. a decrease of 40.24%, 50.51% and 6.9% in the same order. We can therefore see that the addition of potassium would be an important means of reducing the electrophilicity of our molecule. With regard to the nucleophilic character of our compounds, we find that they take the opposite path to electrophilicity, whatever the level of theory chosen. As for the maximum

charge transfer ΔNmax, which is the capacity of a molecular system to acquire an additional charge [21], we find that this value is higher for compounds C and F. At the B3LYP level of theory, when we compare the value 2.640 obtained for our undoped molecule D0 [20], with 5.257 and 6.285 obtained by C and F respectively, we find an increase of 99.13% and 138.1% over the initial value due to mixed doping, which would have had a direct impact on the reactivity of C and F and consequently conferred on them a very good capacity to acquire additional electronic charges. Based on our results, we suggest that our new dibenzo[b,def]chrysene-doped molecules could be good candidates for the manufacture of devices with photovoltaic applications and also for the fabrication of organic light-emitting diodes (OLEDs).

Linear and non-linear optical properties

The linear and non-linear optical properties of molecules now play a key role in establishing molecular structure and assembling organic materials. Understanding non-linear optical properties underpins advances in current technologies such as telecommunication, optical switching, signal processing, electro-optical modulation in data storage, and computing processes [91–95]. Interactions of electromagnetic fields with other media are the primary cause of non-linear optical effects, which modify the characteristics of incident fields such as amplitude, frequency or other aspects of propagation [96]. Using the DFT method, we have investigated certain linear and non-linear optical properties of doped derivatives of dibenzo[b,def]chrysene with the 6–311 + + G(d,p) basis set. The properties calculated are: dipole moment (μ), average polarizability $\langle a \rangle$, polarization anisotropy (Δα), molar refractivity (MR), first-order hyperpolarizability (β_{mol}) and second-order hyperpolarizability (γ). Table 3 summarizes the values of these parameters calculated at the B3LYP and CAM-B3LYP levels of theory, and shows in general that the non-linear optical properties decrease considerably from B3LYP to CAM-B3LYP, while the linear optical parameters vary very little. Thus, polarizability values vary according to the following order A < B < C < D < E < F whatever the method used except for compound C with CAM-B3LYP, i.e. a decrease of 6%, 5.84%, 9.2%, 12.93%, 12.90% and 16.61% respectively for A, B, C, D, E and F Depending on whether we vary from B3LYP to CAM-B3LYP. The values of molar refractivity (MR) at the B3LYP level of theory follow much the same pattern, but this changes with CAM-B3LYP, where we obtain instead A < B < D < E < C < F and the percentage reductions of 6.4%, 5.84%, 9.26%, 12.94%, 12.90% et 16.62% respectively for A, B, D, E, C and F when we move from the B3LYP level of theory to the CAM-B3LYP level of theory 6.4%, 5.84%, 9.26%, 12.94%, 12.90% and 16.62%. The anisotropy of polarizability accounts for the optical dependence of the

Table 3 Total dipole moment μ_{tot}, average polarizability $\langle a \rangle$, anisotropy of polarizability Δa, molar refractivity MR, the first order static hyperpolarizability β and the second order static hyperpolarizability γ of dibenzo[b,def]chrysene derivatives (A, B, C, D, E and F), obtained at the CAM-B3LYP and B3LYP levels of theory with 6–311 + + G(d,p) basis set

Methods	B3LYP						CAM-B3LYP					
Molecules /properties	A	B	C	D	E	F	A	B	C	D	E	F
μ_{tot}(Debye)	7.101	3.884	9.853	15.897	14.110	23.270	6.750	3.873	8.940	16.557	11.975	19.990
$\langle \alpha \rangle (\times 10^{-24}$esu)	55.188	55.907	70.882	73.712	73.787	94.125	51.613	52.640	64.314	64.177	64.269	78.486
$\Delta\alpha (\times 10^{-24}$esu)	71.895	70.963	96.610	94.199	82.909	125.128	63.755	63.865	80.520	75.605	69.274	93.240
MR(esu/mol)	139.164	140.978	178.740	185.876	186.064	237.350	130.150	132.740	162.178	161.833	162.063	197.914
$\beta_{mol} (\times 10^{-30}$esu)	50.247	16.492	229.993	178.750	167.727	420.615	26.448	9.922	92.088	86.977	51.796	129.449
$\gamma (\times 10^{-36}$esu)	208.756	147.160	967.671	1774.305	949.075	4123.108	121.562	105.451	334.239	383.076	589.472	1145.651

direction of polarizability. For our compounds, we obtained values of 71.895×10^{-24}esu, 70.963, 96.610, 94.199, 82.909 and 125.128×10^{-24}esu for A, B, C, D, E and F respectively. For A, B, C, D, E and F respectively, we obtain an increase in polarizability anisotropy value of the order of 17.1%, 15.57%, 57.34%, 53.41%, 35.03% and 103.78% at the B3LYP level of theory, and 13.72%, 13.92%, 43.63%, 34.86%, 23.57% and 66.32% at the CAM-B3LYP level of theory. Overall, this percentage is higher for compounds C doped with tricyanoethenyl and F doped with tricyanoethenyl and two potassiums. This would appear to be due to the fact that these two molecules are the most reactive, with a great facility for releasing their electrons. Doping considerably increase the anisotropy of the polarizability of the pristine molecule, especially for compound F, whose percentage is over 100%, i.e. more than double the value of the initial D0 molecule.

The dipole moment is a measure of a molecule's polarity. For a molecule to be polar, it must have at least one polarized bond, and the barycenter of the negative charges must not coincide with that of the positive charges. We obtained the values $\mu = 7.101$ Debye, 3.884, 9.853, 15.897, 14.110 and 23.270 Debye with B3LYP and 6.750 Debye, 3.873, 8.940, 16.557, 11.975 and 19.990 Debye with CAM-B3LYP respectively for A, B, C, D, E and F, i.e. a very satisfactory increase in this magnitude which was zero for the undoped molecule and unsuitable for NLO applications. Doping has thus enabled us to design new molecules in which the charge distribution is non-centrosymmetric, which could then have excellent NLO responses. First-order static hyperpolarizability is a central parameter with regard to the nonlinear optical behavior of organic materials. The highest β_{mol} values for both doping types obtained with B3LYP are 229.993×10^{-30}esu and 420.615×10^{-30}esu, and those obtained with CAM-B3LYP are 92.088×10^{-30}esu and 129.449×10^{-30}esu for C and F respectively. These previous values obtained with CAM-B3LYP are 99.23 times and 140 times higher than urea [97] on the one hand, 10 times and 14 times higher than para-nitroaniline [98] on the other hand. From the calculated HOMO–LUMO energy values we find that compounds with low gap energy values are those with the highest first-order static hyperpolarizability values which enhances the NLO response of doped dibenzo[b,def] chrysene derivatives. Hence, our new molecules could be very good candidates for non-linear optics (NLO) applications. Similarly, the highest values of second-order hyperpolarizability γ of our molecules doped with B3LYP are 967.6×10^{-36}esu for C et 4123.108×10^{-36}esu for F respectively for doping with organic dopants and mixed doping. With CAM-B3LYP we obtained 334.239×10^{-36}esu for C et 1145.651×10^{-36}esu for F. Comparing our results with the value of $\gamma = 48 \times 10^{-36}$esu obtained for urea, we find that our compounds are at least 2 to 86 times superior to urea.

We carried out frequency-dependent simulations for an extended study of NLO properties in dynamic mode and also to assess as far as possible whether the designed doped derivatives could be used under laser working conditions. Table 4 summarizes the parameter values calculated here in this case. The hyperpolarizability coefficients for EOPE (electro-optic Pockel effect) β(-ω, ω, 0) and SHG (second harmonic generation) β(-2ω, ω,ω), were calculated under an incident laser wavelength of 1064 nm and the obtained values of these coefficients are higher than those of the first-order static hyperpolarizability for all doped molecules. We find that the values of the coefficients of the electro-optical Pockel effect (EOPE) are higher for compounds C and F resulting from doping with organic dopants and mixed doping respectively, namely 708.169×10^{-30}esu and 506.334×10^{-30}esu obtained with B3LYP and 125.788×10^{-30}esu and 234.560×10^{-30}esu obtained with CAM-B3LYP. As for the coefficients of second harmonic generation (SHG) we obtained the effect of the nitro group was strongly felt for compound A which gives us the largest value $\beta(-2\,\omega, \omega, \omega) = 526.306 \times 10^{-30}$esu for doping with organic dopants and compound F again for mixed doping with the value $\beta(-2\omega, \omega,\omega) = 13449.925 \times 10^{-30}$esu with B3LYP and with CAM-B3LYP we obtain the highest value with E i.e. $\beta(-2\omega, \omega,\omega) = 280.008 \times 10^{-30}$esu which shows that the amide group plus the two potassiums had a more favorable effect on our initial compound and for doping with organic dopants, it's compound C that will again give us the highest value i.e. $\beta(-2\omega, \omega,\omega) = 506.262 \times 10^{-30}$esu. It has recently been established that hyper-Rayleigh scattering is an interesting technique for calculating first-order hyperpolarizability, both theoretically and practically [99]. In view of the vital role this technique plays in the design of new materials, frequency doubling, high-resolution microscopy and fast electro-optical modulation [100], hyper-Rayleigh scattering has become indispensable for in-depth study of the NLO properties of organic materials. The highest $\beta_{HRS}(-2\,\omega, \omega, \omega)$ values obtained with B3LYP for doping with organic dopants is 200.614×10^{-30}esu for A and for mixed doping is 4794.824×10^{-30}esu for F i.e. an increase of 2290% compared to the value for compound A. This shows that the substitution of the two potassiums has a positive influence on the NLO behavior of our initial molecule. With CAM-B3LYP, on the other hand, these values drop considerably, obtaining values of 213.365×10^{-30}esu for C 130.600×10^{-30}esu for F respectively for the two types of doping. The depolarization ratio DR is an important parameter for determining the geometry of our doped molecules. When DR is less than 4.5 we are in the case of an octupolar contribution, and if DR is greater than 4.5 we are in the case of a dipolar contribution [101]. At the B3LYP level of theory, the DR values for compounds B and E are 4.839 and 5.678 respectively, i.e. these two molecules have an octupolar contribution, and for

Table 4 Estimated values of frequency dependent NLO response at 1064 nm for dibenzo[b,def]chrysene molecule: EOPE coefficient β(-ω,ω,0), first order hyperpolarizability β(-2ω,ω,ω), HRS response β_{HRS}(-2ω, ω, ω), depolarization ratio DR, dc-kerr effect γ(-ω;ω,0,0), second order hyperpolarizability γ(-2ω;ω,ω,0), degenerate four-wave mixing of the third-order NLO response γ^{DFWM}, and nonlinear refractive index n_2 at B3LYP and CAM-B3LYP levels of theory with 6–311 + + G(d,p) basis set given by A, B, C, D, E and F

Methods	B3LYP						CAM-B3LYP					
Molecules /properties	A	B	C	D	E	F	A	B	C	D	E	F
$\beta(-\omega, \omega, 0)$ ($\times 10^{-30}$esu)	65.808	19.493	708.169	297.429	310.296	506.333	30.711	11.593	125.788	118.326	75.250	234.559
$\beta(-2\ \omega, \omega,\omega)$ ($\times 10^{-30}$esu)	526.306	26.615	469.151	6091.682	9695.203	13,449.925	46.426	16.022	506.261	274.026	280.008	212.269
DR	0.365	4.839	2.973	2.315	5.678	4.398	5.293	3.709	4.384	1.029	3.490	0.717
β_{HRS}(-2 ω, ω, ω) ($\times 10^{-30}$esu)	200.614	11.202	185.900	2710.475	3877.518	4794.824	19.752	5.912	213.365	103.396	112.630	130.600
$\gamma(-2\omega, \omega, \omega, 0)$($\times 10^{-36}$esu)	17,596.285	221.344	2190.523	-617,737.015	5,474,072.772	1,801,468.338	256.192	291.965	9864.903	5364.585	3922.707	5034.211
$\gamma(-\omega, \omega, 0,0)$($\times 10^{-36}$esu)	330.833	189.14	9845.189	3086.109	3149.980	15,627.537	153.368	127.838	554.492	1313.536	897.412	2717.74
γ^{DFWM}($\times 10^{-36}$esu)	6126.677	166.470	10,252.810	-203,417.664	1,827,524.546	614,742.614	198.245	190.011	3731.380	2974.040	2008.49	4013.928
n_2($\times 10^{-20}$ m^2/W)	10.100	0.274	16.900	-334.00	3000	1010	0.326	0.312	6.13	4.89	3.30	6.60

the other compounds A, C, D and F we obtain 0.365, 2.973, 2.315 and 4.398 respectively, i.e. a dipolar contribution. At the CAM-B3LYP level of theory, apart from compound A for which DR = 5.293, thus exhibiting an octupolar contribution, the other five molecules have a dipolar contribution because DR is less than 4.5.

We have also calculated second-order hyperpolarizability, and third-order NLO coefficients, such as EOPE $\gamma(-\omega, \omega, 0,0)$ and EFISHG (electric-field-induced second-harmonic generation) $\gamma(-2\omega, \omega, \omega, 0)$ at wavelength 1064 nm the values of these parameters are also contained in Table 4. At the CAM-B3LYP level of theory the highest values of $\gamma(-\omega, \omega, 0,0)$ are 554.492×10^{-36}esu for C and 2717.74×10^{-36}esu for F obtained and at the B3LYP level we obtained 9845.189×10^{-36}esu for C and 15,627. 537×10^{-36}esu for F as the largest values, i.e. an increase of 1675.53% and 475% in the $\gamma(-\omega, \omega, 0,0)$ values of for compounds C and F respectively when going from CAM-B3LYP to B3LYP. These results reveal that the electro-optical Pockel effect of our molecules is very significant, and that this would also be influenced by the conductivity and reactivity of our compounds, which are more pronounced for C and F. On the other hand, with regard to EFISHG, at CAM-B3LYP level of theory we obtained 9864.903×10^{-36}esu for C and 5364.585×10^{-36}esu for D, which are the maximum values, while at B3LYP level of theory we obtained 17,596. 285×10^{-36}esu given by A and $5,474,072.772 \times 10^{-36}$esu given by E. Contrary to the observation made for the EOPE coefficients here the evolution is complex in view of compounds A, D and E which show us rather a more intense EFISHG behavior. We have evaluated the quadratic nonlinear refractive index (n_2) of our various doped compounds, with a view to making more precise statements about their fields of application. Materials with NLO response and improved non-linear quadratic refractive indices are known to have potential applications in optoelectronics as wavelength converters, optical pulse modulators and optical switches [102]. The values of this quantity summarized in Table 4 were calculated by Eq. (13) from the degenerate four-wave mixture. We find that n_2 is maximum for compounds C (6.13×10^{-20} m^2/W) and F (6.60×10^{-20} m^2/W) at the CAM-B3LYP level of theory, this will change at the B3LYP level of theory with maximum values given by C (16.9×10^{-20} m^2/W) and E (3000×10^{-20} m^2/W). Our maximum values obtained with CAM-B3LYP are at least 2.24 times higher than the $n_2 = (2.74 \pm 0.17) \times 10^{-20}$ m^2/W value obtained for fused silica [103], and 0.023 times lower than the $n_2 = (2.6 \pm 0.6) \times 10^{-18}$ m^2/W value obtained from experiments carried out in the CS2 liquid [104] often taken as a reference for degenerate four-wave mixing. Compared with the maximum values obtained with the B3LYP functional, we find that this CS2 liquid value is 11.54 times smaller than the E value. We therefore suggest that materials

C, E and F, in addition to having proven their potential NLO abilities in the static mode, should have a wider NLO application field than the six studied. On the other hand, γ^{DFWM} which is a four-wave degreed mixture with third-order NLO response evolves along the same order as n_2 because the parameters are linearly related.

Electrical susceptibility

Susceptibility is a parameter that characterizes the polarization created by an electric field, i.e. a material's ability to destroy its own electron cloud. This deformation of the electronic cloud thus gives rise to the modification of certain parameters such as the phase and polarization of the incident light, the frequency, and so on [67]. We have calculated the average first-order susceptibility using Eq. (14), and the values are summarized in Table 5. From table S.13 in supplementary materials, it emerges that $\chi_{xx}^{(1)}$ and $\chi_{yy}^{(1)}$ are the highest components of the first-order susceptibility tensor whatever the level of theory used. The maximum values 4.448 and 5.244 for the average electrical susceptibility $\chi_{tot}^{(1)}$ of the six compounds are given by C and D from organic and mixed doping respectively at the B3LYP level of theory. These values reduce with the CAM-B3LYP level of theory, with maximum values of 4.093 given by A and 4.895 given by D. This represents a 7.13% increase in the susceptibility value of compound D when moving from the CAM-B3LYP to the B3LYP level of theory. These results make our new molecules potential materials for optical applications. Furthermore, we have summarized in Table 5, the values of the second-order susceptibility calculations $\chi^{(2)}(-2\omega, \omega, \omega)$ and that of the linear electro-optic susceptibility $\chi^{\mathrm{LEO}}(\omega)$, and that of the third-order susceptibility $\chi^{(3)}(-2\omega, \omega, \omega, 0)$, the electro-optic dc-Kerr $\chi^{\mathrm{dc-Kerr}}(\omega)$ and the degenerate four-wave mixing of the third-order NLO response χ^{DFWM} in frequency-dependent dynamic mode under the laser wavelength of 1064 nm. The values of these parameters were obtained using Eq. (14). The second-order susceptibility still or second harmonic generation response is maximal for compounds A (6.523×10^{-10} mV^{-1}) and compounds F (100.314×10^{-10} mV^{-1}) with B3LYP, followed by compounds C (4.767×10^{-10} mV^{-1}) and D (3.489×10^{-10} mV^{-1}) at the CAM-B3LYP level of theory. When we compare our $\chi^{(2)}(-2\omega, \omega, \omega)$ results overall, to that of quartz which is the reference for materials with second harmonic generation (SHG) [105] effects whose value is 1 pm/V we find that our materials have values at least 18. 7 times higher than quartz in the case of compound B at the CAMAB3LYP level with $\chi^{(2)}(-2\omega, \omega, \omega)=0.187\times10^{-10}$ mV^{-1} and at most 476.7 times higher in the case of compound C at the same level of theory. However, our calculations show that the electro-optical susceptibility $\chi^{\mathrm{LEO}}(\omega)$ is rather higher for C (1.185×10^{-10} mV^{-1}) and F (1.687×10^{-10} mV^{-1}) at the CAM-B3LYP level of theory, which increases at the B3LYP level where C (7.413×10^{-10} mV^{-1}) and F (3.776×10^{-10} mV^{-1}) give the maximum values. The electro-optical dc-Kerr effect $\chi^{\mathrm{dc-Kerr}}(\omega)$ is also maximal for compounds C and F at the theoretical levels. We thus find here that the linear electro-optic susceptibility $\chi^{\mathrm{LEO}}(\omega)$ and the electro-optic dc-Kerr $\chi^{\mathrm{dc-Kerr}}(\omega)$ increase as the gap energy decreases, which would be at the origin of the increase in the semiconducting character of our C and F materials and also of their reactivity.

The third-order susceptibility $\chi^{(3)}(-2\omega, \omega, \omega, 0)$, or third harmonic generation (THG) response has been calculated and the values obtained show very good consistency with the literature. When compared with the $\chi^{(3)}(-2\omega, \omega, \omega, 0)=2\times10^{-22}$ m^2V^{-2} value of silica, which is the reference material for third harmonic generation [106, 107], we find a percentage increase ranging from 1785% to 51,560% compared with the reference value at the CAM-B3LYP level of theory. This interval is wider at the B3LYP level of theory, with the highest values given by A (24.25×10^{-20} m^2V^{-2}) and E (5458.457×10^{-20} m^2V^{-2}). Finally, the degenerate four-wave mixture of the third-order NLO response χ^{DFWM}, at the CAM-B3LYP level of theory, we have the maximum

Table 5 Average static electric susceptibility ($\chi_{\mathrm{tot}}^{(1)}$), frequency-dependent second order susceptibility $\chi^{(2)}(-2\omega, \omega, \omega)$, Linear electro-optic susceptibility $\chi^{\mathrm{LEO}}(\omega)$ and third order susceptibility $\chi^{(3)}(-2\omega, \omega, \omega, 0)$, EOPE dc-kerr effect $\chi_{\mathrm{T}}^{\mathrm{dc-kerr}}(\omega)$, degenerate four-wave mixture of third order response $\chi^{\mathrm{DFWM}}(\omega)$ values at $\omega=1064$ nm for dibenzo[b,def]chrysene doped derivatives (A, B, C, D, E and F) at B3LYP and CAM-B3LYP level of the theory

Methods	B3LYP						CAM-B3LYP					
Molecules /properties	A	B	C	D	E	F	A	B	C	D	E	F
$\chi_{tot}^{(1)}$	4.102	4.233	4.448	5.244	3.962	4.207	4.093	3.690	3.635	4.895	4.453	3.390
$\chi^{(2)}(-2\omega, \omega, \omega)$ (10^{-10} mV^{-1})	6.523	0.337	4.911	72.334	86.945	100.314	0.615	0.187	4.767	3.489	3.237	1.526
$\chi^{LEO}(\omega)$ (10^{-10} mV^{-1})	0.816	0.147	7.413	3.532	2.783	3.776	0.407	0.135	1.185	1.507	0.870	1.687
$\chi^{(3)}(-2\omega, \omega, \omega, 0)$ (10^{-20} m^2V^{-2})	24.250	0.312	2.550	-719.047	5458.457	1493.958	0.377	0.379	10.332	7.595	5.042	4.026
$\chi_T^{dc-kerr}(\omega)$(10^{-20} m^2V^{-2})	0.456	0.180	11.460	4.075	3.141	12.960	0.226	0.166	0.581	1.860	1.153	2.173
$\chi^{DFWM}(\omega)$(10^{-20} m^2V^{-2})	8.443	0.234	11.934	-268.572	1822.311	509.806	0.292	0.2464	3.908	4.210	2.581	3.209

values 3.908×10^{-20} m^2V^{-2} for C and 3.209×10^{-20} m^2V^{-2} for D for organic and mixed doping respectively. The reference value for the degenerate four-wave mixture of the NLO response is silica with $\chi^{DFWM} = 2.04 \times 10^{-22}$ m^2V^{-2} [103], comparing this value with those obtained for C and D we find an increase of 19,057% and 15,630% respectively over the reference material, making our molecules potential candidates for applications in the field of nonlinear optics.

Thermodynamic properties

We have selected and evaluated at normal pressure (1 atm) and room temperature (298. 150 °K) certain thermodynamic properties of doped dibenzo[b,def]chrysene derivatives (A, B, C, D, E and F), such as electronic energy without zero-point correction (Eel), zero-point vibrational energy (ZPVE), sum of electronic energies with zero-point correction (E_0), the sum of electronic and thermal energies (E), enthalpy (H), the sum of electronic and thermal free energies (G), the contribution of thermal energy correction (Eth), heat capacity (Cv) and entropy (S). In Table 6, we have grouped together all the calculated parameter values. We note that the values of Eel, ZPVE, E0, E, H, G, and Eth increase as we move from mixed doping to doping with organic dopants and to the virgin molecule D0 [20], i.e. from D to A, from E to B and from F to C with the maximum value obtained by D0. Already in our previous work, we had the best results for thermodynamic properties using the B3LYP level of theory and our current results don't say otherwise, so we'll discuss more of our results using this level of theory.

With regard to the values obtained for the enthalpies (H) and Gibbs free enthalpies (G), they are all negative, implying that our molecules are thermodynamically stable. At the B3LYP level of theory, we obtained the lowest values for doping with organic dopants with compound C, i.e. $H = -801.386 \times 10^3$ (kcal/Mol) and $G = -801.435 \times 10^3$(kcal/Mol), and the highest values with B, i.e. $H = -685.027 \times 10^3$ (kcal/Mol) and $G = -685.069 \times 10^3$ (kcal/Mol). Substituting two hydrogens from A, B and C with two potassiums reduces H and G values by 109.8%, 106.3% and 93.85% respectively when moving from A to D, B to E and C to F. Thus, C is the most stable molecule obtained in the case of doping with organic dopants, and C is also less stable than F, which is the most stable of all six compounds due to its lower G free energy value.

Thermal energy can be assimilated to the kinetic energy resulting from the movements of the atoms or molecules of a given body. Our results show that, at both levels of theory, this quantity increases in the order A < B < C, in the case of doping with organic dopants, and D < E < F, in the case of mixed doping. The highest value is given by C, i.e. $E_{th} = 220.350$ kcal/Mol, and the lowest by D, i.e. $E_{th} = 187.393$ kcal/Mol, obtained with B3LYP, so we can say that the stability of our compounds varies with the two types of doping carried out. The entropy of a molecular system is the physical quantity that measures its degree of disorder. Cv is the amount of thermal energy required to raise a system's

Table 6 Total electronic energy without zero-point correction (E_{el}), zero point vibrational energy (ZPVE), sum of electronic energy with zero-point correction (E_0), sum of electronic and thermal Energies (E), enthalpies (H), sum of electronic and thermal free energies (G), thermal energy correction contribution (E_{th}), constant volume molar heat capacity (C_v) and the entropy (S) of dibenzo[b,def]chrysene derivatives (A, B, C, D, E and F), obtained at the CAM-B3LYP and B3LYP levels of theory with 6–311 + + G(d,p) basis set

Methods	B3LYP					
Molecules /properties	A	B	C	D	E	F
$E_{el} \times 10^3$(kcal/Mol)	-707.712	-685.244	-801.607	-1459.831	-1437.369	-1553.736
ZPVE (kcal/Mol)	189.022	204.412	205.608	172.946	188.115	189.365
$E_0 \times 10^3$(kcal/Mol)	-707.522	-685.039	-801.401	-1459.660	-1437.181	-1553.546
$E \times 10^3$(kcal/Mol)	-707.511	-685.027	-801.386	-1459.644	-1437.166	-1553.529
$H \times 10^3$(kcal/Mol)	-707.510	-685.027	-801.386	-1459.643	-1437.165	-1553.528
$G \times 10^3$(kcal/Mol)	-707.552	-685.069	-801.435	-1459.694	-1437.217	-1553.586
E_{th} (kcal/Mol)	200.558	216.390	220.350	187.393	202.983	206.968
Cv(cal/Mol$^-$Kelvin)	77.415	80.792	94.854	87.902	91.263	105.292
S (cal/Mol$^-$Kelvin)	138.970	141.139	164.457	169.504	174.009	196.184
Methods	CAM-B3LYP					
$E_{el} \times 10^3$(kcal/Mol)	-707.334	-684.866	-801.161	-1459.467	-1437.004	-1553.303
ZPVE (kcal/Mol)	191.839	207.261	208.76464	175.809	190.942	192.452
$E_0 \times 10^3$(kcal/Mol)	-707.142	-684.660	-800.952	-1459.291	-1436.813	-1553.110
$E \times 10^3$(kcal/Mol)	-707.131	-684.647	-800.937	-1459.276	-1436.798	-1553.093
$H \times 10^3$(kcal/Mol)	-707.130	-684.647	-800.937	-1459.276	-1436.798	-1553.092
$G \times 10^3$(kcal/Mol)	-707.171	-684.688	-800.986	-1459.326	-1436.849	-1553.151
E_{th} (kcal/Mol)	203.194	219.065	223.292	190.059	205.595	209.836
Cv(cal/Mol$^-$Kelvin)	76.057	79.462	93.381	86.469	89.860	103.759
S (cal/Mol$^-$Kelvin)	138.000	140.141	162.951	168.492	172.174	195.835

temperature by one Kelvin. The values of these parameters increase from A to C and from D to F for both types of doping, and it can be seen that compounds C and F are the ones that require the most energy for a temperature rise, and are also the compounds that are in the most disordered states possible. This confirms once again that these two molecules are the most stable.

Absorption analysis

We have carried out TD-DFT simulations to calculate the absorption properties of doped dibenzo[b,def]chrysene derivatives designed with the 6-311G + + (d,p) basis set in the gas phase, also to verify the transparency of our compounds for potential applications in laser technology, organic solar panel design, light emitters and receivers [64],. According to the work of S. Hirata et al. [108], TD-DFT calculations have been proven to reproduce the excitation energies of the low-lying valence excited states of open and closed-shell PAHs with an accuracy of 0.3 eV plus or minus, and qualitatively adequate oscillator strengths. In our calculations we restricted ourselves to the first six electron transitions and singlet states, then calculated parameters such as excitation energy (E), oscillator strengths (f) and observed transition wavelength (λ) while giving the major contributions of each excitation state. All calculated parameters are summarized in Table 7. All absorption wavelength maxima of our compounds are longer than that of pure dibenzo[b,def] chrysene D0 (307 nm) [20], so that all absorption spectra show a bathochromic shift with respect to D0. The UV–vis spectra are shown in Fig. 7, with absorbances (ε) on the left and oscillator strengths (f) on the right, and wavelengths (λ) on the abscissa. Overall, we can see that the wavelength values evolve in the opposite direction to the excitation energy E. Therefore, we will focus on the longer wavelengths corresponding to very low excitation energies, with a view to reducing the conduction band to facilitate the transition of electrons from the ground state to the excited state.

We based our work on the experimental work of H. Wang et al. [40], who evaluated the absorption spectrum of our initial molecule in argon. Their experiments yielded a maximum wavelength λ = 438.8 nm, which was assigned to the S1—> S0 transition with excitation energy E = 2.83 eV, and another wavelength λ = 305.5 nm corresponding to a considerable absorption peak with transition energy E = 4.06 eV.

Compound A doped with the nitro group absorbs at a wavelength of 333.38 nm with an oscillator strength f = 0.57 and a combined contribution of H-1- > LUMO (34%), H-1- > L + 1 (44%), HOMO- > L + 3 (10%), HOMO- > L + 1 (3%), HOMO- > L + 2 (3%), to which an energy of 3.72 eV a is associated located in the ultraviolet region and an absorbance of the order of 45,000. Here we can observe a second, equally significant peak, this time belonging to the visible range at wavelength λ = 443.62 nm, oscillator strength f = 0.26, contribution HOMO- > L + 1 (86%), H-1- > LUMO (9%), HOMO- > LUMO (4%) with excitation energy E = 2.79 eV and absorbance of the order of 20,000, i.e. a decrease in absorbance and oscillator strength by more than half compared with the first peak. We find that the results of our TD-DFT calculations are in good agreement with the experimental values and as close to the predicted values of 2.6 – 2.9 eV for the main transition energy as the values of H. Wang et al. [40].

When we substitute two hydrogens of the previous compound A by two potassiums we obtain the new compound D. From the data in Table 7 and Fig. 7 we note the presence of the maximum peak at wavelength λ = 525.63 nm, an oscillator strength f = 0. 49 with major contributions from HOMO- > LUMO (85%), H-1- > L + 1 (2%), HOMO- > L + 3 (9%) associated with energy E = 2.15 eV and absorbance equal to that of A. We note a considerable decrease in the energy value with the second doping, i.e. 1.57 eV less compared to the value obtained for the main peak with compound A doped with nitro only. The wavelength has also increased by 192.25 nm compared with A. Here we see a very significant bathochromic effect due to the addition of excess electrons.

Compound B, on the other hand, is derived from the doping of our pristine molecule with the amide group. The maximum absorption peak is observed at wavelength λ = 310.08 nm, corresponding to the ultraviolet range, with an oscillator strength f = 0.68 and corresponding to a combined major contribution H-1- > LUMO (26%), HOMO- > L + 2 (10%), HOMO- > L + 3 (34%), H-4- > LUMO (5%), H-2- > LUMO (5%), HOMO- > L + 1 (9%), HOMO- > L + 4 (3%). This transition is associated with energy E = 4.00 eV, i.e. a difference of 0.03 eV compared with D0, and the absorbance here is of the order of 72,000, i.e. 18,000 less than D0, giving a hypochromic effect. Then we obtain a secondary wavelength of 474.71 nm for the second significant peak belonging to the visible light spectrum, with an oscillator strength f = 0.17 and a combined transition HOMO- > LUMO (96%), HOMO- > L + 1 (2%) associated with energy 2.61 eV and an absorbance rather of the order of 13,000. When we replace two hydrogens in B with two potassiums, we obtain compound E. Figure 7d of the absorption spectrum of E shows a single peak and intense absorption bands. At wavelength λ = 544.38 nm corresponds the maximum absorption with the combined action of the transitions H-1- > LUMO (88%) and HOMO- > L + 2 (8%) and an intensity f = 0.34 then secondary band located at length λ = 524.68 nm which corresponds to the combined transition of H-2- > L + 1 (49%) and HOMO- > L + 2 (45%), the intensity of the oscillator force is f = 0.29. Our molecule absorbs totally in the visible range, and both the undoped

Table 7 Single-Singlet permitted excitation energies (E), absorption wavelength (λ), oscillator strength (f) and major contributions of dibenzo[b,def]chrysene doped derivatives (A, B, C, D, E and F) obtained using TD-DFT at B3LYP level of theory with 6–311 + + G(d,p) basis set

Molecules	A				B			
Excited state	E(eV)	λ(nm)	f	Major contribution	E(eV)	λ(nm)	f	Major contribution
1	2.29	541.32	0.02	HOMO->LUMO (95%) HOMO->L+1 (4%)	2.61	474.71	0.17	HOMO->LUMO (96%)HOMO->L+1 (2%)
2	2.79	443.62	0.26	HOMO->L+1 (86%), H-1->LUMO (9%), HOMO->LUMO (4%)	3.08	402.48	0.07	H-1->LUMO (31%), HOMO->L+1 (66%)
3	3.36	369.17	0.17	H-1->LUMO (38%), HOMO->L+2 (37%), HOMO->L+3 (11%), H-1->L+1 (8%), HOMO->L+1 (5%)	3.48	356.28	0.02	H-2->LUMO (14%), HOMO->L+2 (78%)H-1->LUMO (2%), HOMO->L+1 (3%)
4	3.55	349.42	0.05	H-1->LUMO (38%), HOMO->L+2 (37%), HOMO->L+3 (11%), H-1->L+1 (8%), HOMO->L+1 (5%)	3.77	328.68	0.11	H-2->LUMO (76%) H-1->LUMO (6%), HOMO->L+1 (4%), HOMO->L+2 (7%)
5	3.66	338.41	0.01	H-2->LUMO (49%), HOMO->L+2 (24%), HOMO->L+3 (10%), H-2->L+1 (3%), H-1->LUMO (7%), HOMO->L+4 (4%)	3.80	326.06	0.45	H-1->LUMO (27%), HOMO->L+1 (13%), HOMO->L+3 (46%) H-4->LUMO (6%), HOMO->L+2 (2%)
6	3.72	333.38	0.57	H-1->LUMO (34%), H-1->L+1 (44%), HOMO->L+3 (10%) HOMO->L+1 (3%), HOMO->L+2 (3%)	4.00	310.08	0.68	H-1->LUMO (26%), HOMO->L+2 (10%), HOMO->L+3 (34%) H-4->LUMO (5%), H-2->LUMO (5%), HOMO->L+1 (9%), HOMO->L+4 (3%)
Molecules	**C**				**D**			
1	1.48	839.28	0.03	HOMO->LUMO (99%)	2.15	575.55	0.23	HOMO->LUMO (85%)H-1->L+1 (2%), HOMO->L+3 (9%)
2	2.60	476.67	0.00	H-1->LUMO (45%), HOMO->L+1 (49%)H-2->LUMO (4%)	2.22	556.51	0.00	HOMO->L+1 (97%)
3	2.80	442.29	0.90	H-2->LUMO (12%), H-1->LUMO (51%), HOMO->L+1 (34%)	2.23	555.80	0.00	HOMO->L+2 (96%)
4	2.85	435.14	0.26	H-2->LUMO (82%), HOMO->L+1 (13%)	2.28	543.41	0.00	H-2->LUMO (66%), H-1->LUMO (29%)
5	3.30	376.74	0.05	H-1->L+1 (41%), HOMO->L+2 (56%)	2.35	526.36	0.01	H-2->LUMO (27%), H-1->LUMO (61%)H-1->L+3 (5%)
6	3.38	366.47	0.04	H-3->LUMO (93%)HOMO->L+3 (3%)	2.36	525.63	0.49	H-2->L+1 (10%), H-2->L+2 (27%), H-1->L+1 (45%)H-1->L+2 (7%), HOMO->L+3 (6%)
Molecules	**E**				**F**			
1	1.98	627.10	0.00	HOMO->LUMO (13%), HOMO->L+1 (86%)	0.85	1463.79	0.02	HOMO→LUMO (100%) HOMO->LUMO (99%)
2	1.99	622.60	0.00	HOMO->LUMO (86%), HOMO->L+1 (13%)	1.24	999.84	0.00	H-2->LUMO (93%)H-1->LUMO (7%)
3	2.28	544.38	0.34	H-1->LUMO (88%)HOMO->L+2 (8%)	1.25	988.49	0.00	H-1->LUMO (93%)H-2->LUMO (7%)
4	2.36	524.68	0.29	H-2->L+1 (49%), HOMO->L+2 (45%)	2.11	586.29	0.27	H-3->LUMO (89%)HOMO->L+3 (7%)
5	2.46	503.35	0.01	H-2->L+1 (45%), HOMO->L+2 (41%)H-1->LUMO (8%), HOMO->L+3 (3%)	2.20	563.43	0.30	H-4->LUMO (86%)H-3->LUMO (2%), HOMO->L+2 (8%)
6	2.48	498.96	0.00	H-2->L+2 (96%)	2.20	563.28	0.00	HOMO->L+2 (87%)H-4->LUMO (8%), HOMO->L+1 (4%)

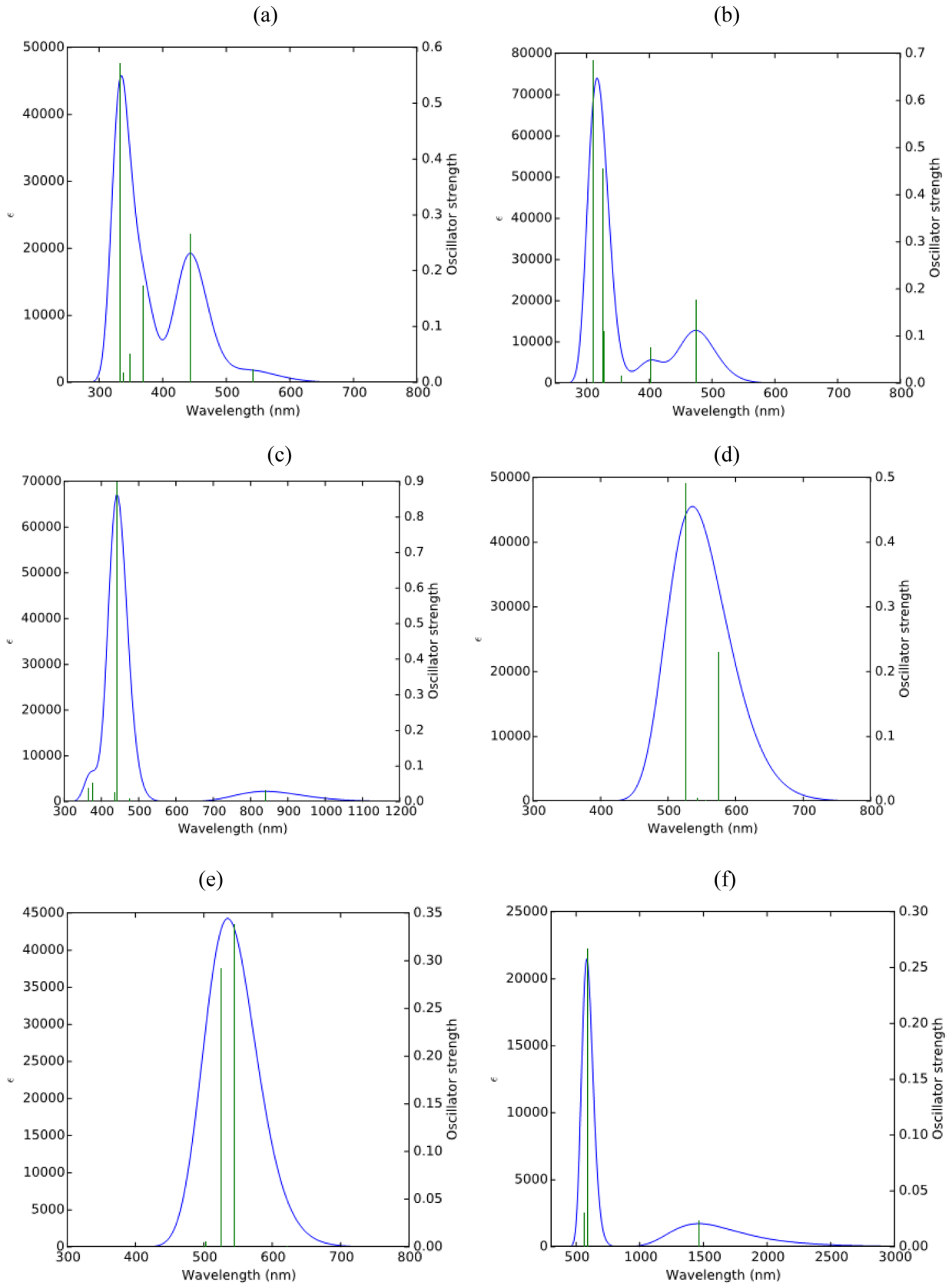

Fig. 7 Absorption spectra by theoretical TD-DFT/B3LYP with the 6–311 + + G(d,p) basis set of dibenzo[b,def]chrysene doped derivatives: (**a**): A, (**b**): B, (**c**): C, (**d**): D, (**e**): E, (**f**): F

D0 [20] molecule and molecule B retain their bathochromic and hypochromic effects.

Doping our pristine molecule with the tricyanoethenyl group produces compound C. Figure 7c of the absorption spectrum of C contains only one intense maximum absorption band at wavelength λ = 442.29 nm, corresponding to the combination of transitions H-2- > LUMO (12%), H-1- > LUMO (51%) and HOMO- > L + 1 (34%) with intensity f = 0.90. With a maximum absorbance of 67,000, the hypochromic effect is therefore maintained in relation to D0. However, if we continue with the substitution of two potassiums for two hydrogens, we obtain compound F, whose UV–vis spectrum is shown in Fig. 7f. Table 7 gives us the wavelength λ = 563.43 nm at which absorption is maximized by the combined transitions of H-4- > LUMO (86%), H-3- > LUMO (2%) and HOMO- > L + 2 (8%) with an oscillator strength f = 0.30, a transition energy E = 2.20 eV and an absorbance of 23,000, which is the smallest of all obtained. In this case, we see a very deep hypochromic effect and the conservation of the bathochromic effect in relation to D0 and C.

In short, we can see that doping, synonymous with the addition of excess electrons to our initial molecule, has contributed to a significant modification of its electronic and geometric structure. As a result, the maximum wavelength of the initial D0 [20] molecule, λ = 307.80 nm, has increased considerably to λ = 563.43 nm for the F molecule, a difference of 255.63 nm corresponding to an 83.05% increase in wavelength from ultraviolet to visible, giving rise to a strong bathochromic effect due to the n-type doping of our undoped molecule. The absorbance of our doped molecules decreases considerably and linearly as we move from D0 to A and D, from D0 to B and E and from C to F, confirming the hypochromic behavior of our compounds. This behavior is most pronounced for molecule F, which has an absorbance of 23,000, whereas compound D0 has an absorbance of 90,000. The energy of the E transition of our doped molecules also decreases from 4.03 eV for D0 [20] to 2.20 eV for F with TD-DFT. This could explain the fact that our doped molecules are more reactive than the initial molecule. We have therefore just designed new materials that are transparent in the ultraviolet range, with a very important role in improving second harmonic generation (SHG) and third harmonic generation (THG) [109]. Our materials can also be used in the design of display devices and organic solar cells.

Conclusion

Doping with organic dopants and mixed alkali metal plus organic dopants was performed on the pristine dibenzo[b,def]chrysene molecule using DFT and TD-DFT methods with the 6–311 + + G(d,p) basis set. Geometrical, vibrational, optoelectronic, electronic, nonlinear optical and thermodynamic properties have been greatly modified. The interaction energies of the doped molecules range from -1553.736 kcal/mol given by F to -685.244 kcal/mol given by B, all of which are negative and confirm that our molecular structures are thermodynamically stable. No negative frequencies were obtained on the IR absorption and Raman scattering spectra, which means that the minima obtained on the surface of the potential energy of our molecules are local minima. The highest peaks in the infrared (IR) absorption spectra of molecules A and D, B and E, C and F are attributed respectively to (C-N) stretching at frequencies 1361.69 and 1375.12 cm^{-1}, (C = O) stretching at frequencies 1743.32 and 1734.79 cm^{-1} and (C = C) stretching at frequencies 1557.49 and 1525.43 cm^{-1}, all accompanied by in-plane angle deformations. Our values agree with those reported in the literature. Theoretical vibrational modes are consistent with those obtained from experiments, with small differences due in particular to experimental conditions and the methods used in our simulations. The study of optoelectronic properties enabled us to obtain refractive index values higher than those of glass, which is the reference material for optoelectronics. This means that our new molecules can be used under very high field conditions, notably with the very high mean electric field values obtained for the C (4.164×10^9 V.m^{-1}) et F (7.410×10^9 V.m^{-1}) molecules at the B3LYP level of theory. In addition, the effects of doping were strongly felt in terms of electronic properties, with a reduction in the gap energy of the pristine molecule of the order of 35.67% to 58.18% when doped with the tricyanoethenyl group (C molecule) and the tricyanoethenyl plus two potassium groups (F molecule) respectively. This considerable lowering of the energy gab value provides ample evidence of the good semiconducting properties of the resulting C and F compounds, as well as their improved reactivity. With regard to NLO properties, we recall that the pristine dibenzo[b,def]chrysene molecule is centrosymmetric, with dipole moment and first-order hyperpolarizability all zero. With the two types of doping carried out here, we now obtain non-centrosymmetric molecules suitable for NLO applications, with in particular the maximum values of first-order hyperpolarizability given by C (92.088×10^{-30}esu) and F (129.449×10^{-30}esu), and those of second-order hyperpolarizability given by C (967.6×10^{-36}esu) and F (4123.108×10^{-36}esu at the CAM-B3LYP level of theory. These values are higher than those of urea, which is the benchmark for organic materials, making our doped molecules prime candidates for potential NLO applications. We evaluated dynamic hyperpolarizabilities at the 1064 nm frequency, second harmonic generation (SHG), and electro-optical Pockel effect (EOPE), hyper-Rayleigh scattering (βHRS) of light, depolarization ratio (DR). The highest values of (β_{HRS}) at the CAM-B3LYP level of theory are $213{,}365 \times 10^{-30}$esu for C and $130{,}600 \times 10^{-30}$esu

for F. The same applies to the other parameters. Second-order hyperpolarizabilities were calculated and third-order NLO coefficients, such as EOPE $\gamma(-\omega, \omega, 0,0)$ and EFISHG $\gamma(-2\omega, \omega, \omega, 0)$, degenerate four-wave mixing and quadratic nonlinear refractive index (n_2). The n_2 refractive index values are higher than that of fused silica, which is the reference in this field. Analysis of the absorption properties showed a very pronounced bathochromic effect with transparency in the deep ultraviolet region. These excellent results pave the way for the development of new materials with enhanced NLO response.

Supplementary Information The online version contains supplementary material available at https://doi.org/10.1007/s00894-024-06026-8.

Acknowledgements This work was supported by Professor Geh Wilson Ejuh and their mentor Emeritus Professor A.N Singh through providing the Gaussian code.

Author's contribution All authors listed have significantly contributed to the development and the writing of this article.

Funding The authors have not disclosed any funding.

Data availability Supplementary content related to this article has been published online.

Declarations

Competing interests The authors declare that there is no conflict of interest as concern this article.

References

1. Sajid H, Ullah F, Yar M, Ayub K, Mahmood T (2020) Superhalogen doping: a new and effective approach to design materials with excellent static and dynamic NLO responses. New J Chem 16358–16369. https://doi.org/10.1039/D0NJ02291h
2. Schenning APHJ, Meijer EW et al. (2005) Supramolecular electronics; nanowires from self-assembled π-conjugated systems, Chem. Commun., (3245-3258). https://doi.org/10.1039/b501804h
3. Arivanandhan M et al (2008) Directional growth of organic NLO crystal by different growth methods: a comparative study by means of XRD, HRXRD and laser damage threshold. J Cryst Growth 4587–4592. https://doi.org/10.1016/j.jcrysgro.2008.08.036
4. Miller MJ, Wei SH, Parker I, Cahalan MD et al. (2002) Two-Photon Imaging of Lymphocyte Motility and Antigen Response in Intact Lymph Node, Science, (1869-1873). https://doi.org/10.1126/science.1070051
5. Iliopoulos K, Krupka O, Gindre D, Sallé M (2010) Reversible two-photon optical data storage in coumarin-based copolymers. J Am Chem Soc 14343–14345. https://doi.org/10.1021/ja1047285
6. Yeh P, Chiou AE, Hong J, Beckwith P, Chang T, et. Khoshnevisan M (1989) Photorefractive Nonlinear Optics And Optical Computing , Opt Eng (328-343) https://doi.org/10.1117/12.7976959
7. Shaaban KM, Schalkoff RJ (1995) Image processing and computer vision algorithm selection and refinement using an operator-assisted meta-algorithm. In: Visual information processing IV, SPIE, pp 77–87. https://doi.org/10.1117/12.212014
8. Wostyn K, Binnemans K, Clays K, Persoons A (2001) Hyper-Rayleigh scattering in the Fourier domain for higher precision: correcting for multiphoton fluorescence with demodulation and phase data. Rev Sci Instrum 3215–3220. https://doi.org/10.1063/1.1384429
9. Arano-Martinez JA, Martínez-González CL, Salazar MI, Torres-Torres C (2022) A Framework for biosensors assisted by multiphoton effects and machine learning. Biosensors Art n° 9. https://doi.org/10.3390/bios12090710
10. Ashwini R, Vijayanand S, Hemapriya J (2017) Photonic potential of haloarchaeal pigment bacteriorhodopsin for future electronics: a review. Curr Microbiol 996–1002. https://doi.org/10.1007/s00284-017-1271-5
11. Ai H, Bu Y, Li P, Sun L (2004) Marked increments of stability and proton affinity of the protonated, zwitterionic glycine induced by the attachment of two excess electrons. J Phys Chem A 4156–4162. https://doi.org/10.1021/jp049405m
12. Ittyachan R, Sagayaraj P (2003) Growth and characterization of a new nonlinear optical l-histidine diphosphate single crystal. J Cryst Growth 553–556. https://doi.org/10.1016/S0022-0248(02)02115-2
13. Sabari Girisun TC, Dhanuskodi S (2010) Tuning the dielectric properties of thiourea analog crystals for efficient nonlinear optical applications. Mater Res Bull 88–91. https://doi.org/10.1016/j.materresbull.2009.09.010
14. Kulshrestha S, Shrivastava AK (2020) Crystal growth and characterization of organic NLO materials and their application in optical devices. AIP Conf Proc 050010. https://doi.org/10.1063/5.0002152
15. Cho MJ, Choi DH, Sullivan PA, Akelaitis AJP, Dalton LR (2008) Recent progress in second-order nonlinear optical polymers and dendrimers. Prog Polym Sci 1013–1058. https://doi.org/10.1016/j.progpolymsci.2008.07.007
16. Nestoros E, Stuparu MC (2018) Corannulene: a molecular bowl of carbon with multifaceted properties and diverse applications. Chem Commun 6503–6519. https://doi.org/10.1039/C8CC02179A
17. Noudem P, Fouejio D, Mveme CDD, Zekeng SS, Fankam Fankam JB (2022) Impact of doping on the optoelectronic, electronic and nonlinear optical properties and on the reactivity of photochromic polymers containing styrylquinoline fragments: Hartree-Fock and DFT study. Heliyon e11491. https://doi.org/10.1016/j.heliyon.2022.e11491
18. Fonkem CC, Ndjaka JMB, Ejuh GW (2020) DFT study of the enhancement of physico-chemical, nonlinear and optoelectronic properties of the 2-cyano-3-[4(diphenylamino) phenyl] acrylic acid molecule by doping with the potassium atom. Bull Mater Sci 228. https://doi.org/10.1007/s12034-020-02175-7
19. Tsukamoto K et al (2019) π-Extension of electron-accepting dithiarubicene with a cyano-substituted electron-withdrawing group and application in air-stable n-channel organic field effect transistors. J Mater Chem C 12610–12618. https://doi.org/10.1039/C9TC04325J
20. Ribouem A Bessong CD, Ottou Abe MT, Ntieche Z, Noudem P, Olinga Mbala GF, Ndjaka JMB (2023) Influence of lithium doping on optoelectronic, electronic, reactivity descriptors, thermodynamic and nonlinear optical properties of dibenzo[b,def] chrysene: insight by a DFT study. Opt Quantum Electron 1–27. https://doi.org/10.1007/s11082-023-05294-7
21. LF Tsague et al (2023) Ab-initio and density functional theory (DFT) computational study of the effect of fluorine on the electronic, optical, thermodynamic, hole and electron transport properties of the circumanthracene molecule. Heliyon e19647. https://doi.org/10.1016/j.heliyon.2023.e19647

22. Bano R et al (2023) Diamondoid as potential nonlinear optical material by superalkali doping: a first principles study. Diam Relat Mater 109826. https://doi.org/10.1016/j.diamond.2023.109826
23. Kosar N et al (2020) Significant nonlinear optical response of alkaline earth metals doped beryllium and magnesium oxide nanocages. Mater Chem Phys 122507. https://doi.org/10.1016/j.matchemphys.2019.122507
24. Rad AS, Ayub K (2018) Nonlinear optical and electronic properties of Cr-, Ni-, and Ti- substituted C20 fullerenes: a quantum-chemical study. Mater Res Bull 399–404. https://doi.org/10.1016/j.materresbull.2017.09.036
25. RK Konidena et al. KRJ Thomas (2014) Selective naked-eye cyanide detection in aqueous media using a carbazole-derived fluorescent dye, RSC Adv, (22902-22910)
26. Ibrahim M, Mahmoud AA (2009) Computational notes on the reactivity of some functional groups. J Comput Theor Nanosci 1523–1526. https://doi.org/10.1166/jctn.2009.1205
27. Obadahun J, Bello KA, Yakubu MK, Abdelmalik AA, Abdulhakeem AA (2023) Synthesis, characterization and photo-electrochemical conversion of 3, 5-Diamino-4-[(E)-(6-Hydroxy-1, 3-Benzothiazol-2-Yl)Diazenyl]-2-(Tricyanoethenyl) Benzoic Acid. ATBU J Sci Technol Educ 11(3):186–193
28. Lucas B, Trigaud T, Videlot-Ackermann C (2012) Organic transistors and phototransistors based on small molecules. Polym Int 374–389. https://doi.org/10.1002/pi.3213
29. Anthony JE (2006) Functionalized acenes and heteroacenes for organic electronics. Chem Rev 5028–5048. https://doi.org/10.1021/cr050966z
30. JE Anthony (2008) The Larger Acenes: Versatile Organic Semiconductors », Angew Chem Int Ed, (452-483)
31. Noudem P, Fouejio D, Mveme CDD, Nya FT, Zekeng SS (2023) Electronic, nonlinear optical, UV–vis and NBO analysis of methyl methacrylate for optoelectronic and optical applications: DFT study and impact of conformation. Spectrochim Acta A Mol Biomol Spectrosc 123267. https://doi.org/10.1016/j.saa.2023.123267
32. Sharif A, Jabeen S, Iqbal S, Iqbal J (2021) Tuning the optoelectronic properties of dibenzochrysene (DBC) based small molecules for organic solar cells. Mater Sci Semicond Process 105689. https://doi.org/10.1016/j.mssp.2021.105689
33. Sun H, Putta A, Billion M (2012) Arene trifluoromethylation: an effective strategy to obtain air-stable n-type organic semiconductors with tunable optoelectronic and electron transfer properties. J Phys Chem A 8015–8022. https://doi.org/10.1021/jp301718j
34. Burke KB et al (2012) Single crystal x-ray, AFM, NEXAFS, and OFET studies on angular polycyclic aromatic silyl-capped 7,14-Bis(ethynyl)dibenzo[b,def]chrysenes. Cryst Growth Des 725–731. https://doi.org/10.1021/cg201020w
35. Winzenberg KN et al (2009) Dibenzo[b,def]chrysene derivatives: solution-processable small molecules that deliver high power-conversion efficiencies in bulk heterojunction solar cells. Chem Mater 5701–5703. https://doi.org/10.1021/cm9028337
36. Zhang L et al (2012) Triisopropylsilylethynyl-functionalized dibenzo[def,mno]chrysene: a solution-processed small molecule for bulk heterojunction solar cells. J Mater Chem 4266–4268. https://doi.org/10.1039/C2JM14998B
37. Dardenne N et al (2017) Tuning optical properties of dibenzochrysenes by functionalization: a many-body perturbation theory study. J Phys Chem 24480–24488. https://doi.org/10.1021/acs.jpcc.7b08601
38. Gagnon F et al (2022) 2,9-Dibenzo[b , def]chrysene as a building block for organic electronics. Mater Adv 599–603. https://doi.org/10.1039/D1MA00799H
39. Shu Y et al (2013) The impact of tetrahedral capping groups and device processing conditions on the crystal packing, thin film features and OFET hole mobility of 7,14-bis(ethynyl) dibenzo[b,def]chrysenes. J Mater Chem C 6299–6307. https://doi.org/10.1039/C3TC31030B
40. Wang H, Szczepanski J, Hirata S, Vala M (2005) Vibrational and electronic absorption spectroscopy of dibenzo[b,def]chrysene and its ions. J Phys Chem A 9737–9746. https://doi.org/10.1021/jp0527960
41. Zhang F-J, Cortez C, Harvey RG (2000) New synthetic approaches to polycyclic aromatic hydrocarbons and their carcinogenic oxidized metabolites: derivatives of benzo[s]picene, benzo[rst]pentaphene, and dibenzo[b,def]chrysene. J Org Chem 3952–3960. https://doi.org/10.1021/jo9918044
42. Fish MJ et al (2013) Gaussian 09, Revision D01, Gaussian, Inc., Wallingford CT
43. Devi G, Buragohain M, Pathak A (2020) DFT study of five-membered ring PAHs. Planet Space Sci 104593. https://doi.org/10.1016/j.pss.2018.09.003
44. Dennington R, Keith J, Millam J (2016) Gauss view, version 6. Semichem Inc, Shawnee
45. AD Becke (1993) A new mixing of Hartree–Fock and local density-functional theories, J Chem Phys, (1372-1377)
46. Vosko SH, Wilk L, Nusair M (1980) Accurate spin-dependent electron liquid correlation energies for local spin density calculations: a critical analysis. Can J Phys 1200–1211. https://doi.org/10.1139/p80-159
47. Perdew JP, Burke K, Wang Y (1996) Generalized gradient approximation for the exchange-correlation hole of a many-electron system. Phys Rev B 16533–16539. https://doi.org/10.1103/PhysRevB.54.16533
48. Lee C, Yang W, Parr RG (1988) Development of the Colle-Salvetti correlation-energy formula into a functional of the electron density. Phys Rev B 785–789. https://doi.org/10.1103/PhysRevB.37.785
49. Bauschlicher CW (1995) A comparison of the accuracy of different functionals. Chem Phys Lett 40–44. https://doi.org/10.1016/0009-2614(95)01089-R
50. Moore BI, Srebro M, Autschbach J (2012) Analysis of optical activity in terms of bonds and lone-pairs: the exceptionally large optical rotation of norbornenone. J Chem Theory Comput 4336–4346. https://doi.org/10.1021/ct300839y
51. Srebro M, Autschbach J (2012) Tuned range-separated time-dependent density functional theory applied to optical rotation. J Chem Theory Comput 245–256. https://doi.org/10.1021/ct200764g
52. T Yanai, DP Tew, et al. NC Handy (2004) A new hybrid exchange–correlation functional using the Coulomb-attenuating method (CAM-B3LYP), Chem Phys Lett, (51-57) https://doi.org/10.1016/j.cplett.2004.06.011
53. R Misra (2017) Tuning of Second-Order Nonlinear Optical Response Properties of Aryl-Substituted Boron-Dipyrromethene Dyes: Unidirectional Charge Transfer Coupled with Structural Tailoring, J Phys Chem C, (5731-5739)
54. Chaudhry AR, Muhammad S, Irfan A, Al-Sehemi AG, Haq BU, Hussain S (2018) Structural, electronic and nonlinear optical properties of novel derivatives of 9,12-diiodo-1,2-dicarba-closo-dodecaborane: density functional theory approach. Z Für Naturforschung A 1037–1045. https://doi.org/10.1515/zna-2018-0123
55. Cai Z-L, Crossley MJ, Reimers JR, Kobayashi R, Amos RD (2006) Density functional theory for charge transfer: the nature of the N-bands of porphyrins and chlorophylls revealed through CAM-B3LYP, CASPT2, and SAC-CI calculations. J Phys Chem B 15624–15632. https://doi.org/10.1021/jp063376t
56. Cai Z-L, Sendt K, Reimers JR (2002) Failure of density-functional theory and time-dependent density-functional theory for large extended systems. J Chem Phys 117:12 5543–5549. https://doi.org/10.1063/1.1501131

57. B Komjáti et al. (2016) Systematic study on the TD-DFT calculated electronic circular dichroism spectra of chiral aromatic nitro compounds: A comparison of B3LYP and CAM-B3LYP », Spectrochimica Acta Part A: Molecular and Biomolecular Spectroscopy, (95-102)
58. Noudem P, Fouejio D, Mveme CDD, Zekeng SS, Tchangnwa Nya F, Ejuh GW (2022) Hartree-Fock and DFT studies of the optoelectronic, thermodynamic, structural and nonlinear optical properties of photochromic polymers containing styrylquinoline fragments. Mater Chem Phys 125883. https://doi.org/10.1016/j.matchemphys.2022.125883
59. Bano R et al (2022) Face specific doping of Janus all-cis-1,2,3,4,5,6-hexafluorocyclohexane with superalkalis and alkaline earth metals leads to enhanced static and dynamic NLO responses. J Phys Chem Solids 110361. https://doi.org/10.1016/j.jpcs.2021.110361
60. Mveme CDD, Tchangnwa Nya F, Ejuh GW, Yossa Kamsi RA, Ndjaka JMB (2020) Density functional theory study of optoelectronic, nonlinear optical, piezoelectric and thermodynamic properties of poly (3,4-ethylenedioxythiophene), poly(3,4-ethylenedioxyselenophene) and their derivatives. Opt Quantum Electron 373. https://doi.org/10.1007/s11082-020-02492-5
61. Ntieche Z, Abe MTO, freidy OMG, Ejuh GW, Ndjaka JMB (2022) Electronic, non-linear optical, optoelectronic, and thermodynamic properties of undoped and doped bis (ethylenedithio) tetraselenafulvalene (BETS) (C10H8S4Se4) molecule: first study using ab initio investigation. J Mol Model 256. https://doi.org/10.1007/s00894-022-05250-4
62. Fankam JB, Ejuh GW, Tchangnwa Nya F, Ndjaka JMB (2020) Theoretical investigation of the molecular structure, vibrational spectra, thermodynamic and nonlinear optical properties of 4, 5-dibromo-2, 7dinitro- fluorescein. Opt Quantum Electron 292. https://doi.org/10.1007/s11082-020-02396-4
63. Houbrechts S, Clays K, Persoons A, Pikramenou Z, Lehn J-M (1996) Hyper-Rayleigh scattering investigation of nitrobenzyl pyridine model compounds for optical modulation of the hyperpolarisability. Chem Phys Lett 485–489. https://doi.org/10.1016/0009-2614(96)00676-8
64. Bano R et al (2022) Lanthanum doped corannulenes with enhanced static and dynamic nonlinear optical properties: a first principle study. Phys B Condens Matter 414088. https://doi.org/10.1016/j.physb.2022.414088
65. Naeem J et al (2022) Assessment of alkali and alkaline earth metals doped cubanes as high-performance nonlinear optical materials by first-principles study. J Sci Adv Mater Devices 100457. https://doi.org/10.1016/j.jsamd.2022.100457
66. Plaquet A et al (2008) In silico optimization of merocyanine-spiropyran compounds as second-order nonlinear optical molecular switches. Phys Chem Chem Phys 6223–6232. https://doi.org/10.1039/B806561F
67. Reis H, Papadopoulos MG, Calaminici P, Jug K, Köster AM (2000) Calculation of macroscopic linear and nonlinear optical susceptibilities for the naphthalene, anthracene and meta-nitroaniline crystals. Chem Phys 359–371. https://doi.org/10.1016/S0301-0104(00)00305-0
68. Rodrigues RFN et al (2017) Solid state characterization and theoretical study of non-linear optical properties of a Fluoro-N-Acylhydrazide derivative. PLOS ONE e0175859. https://doi.org/10.1371/journal.pone.0175859
69. Fankam Fankam JB, Ejuh GW, Nya FT, Ndjaka JMB (2020) Study of electronic structure, optoelectronics, linear and nonlinear optical properties and chemical descriptors of dibromo-dinitrofluorescein isomers in gasphase and solvent media using abinitio and DFT methods. Chin J Phys 461–473. https://doi.org/10.1016/j.cjph.2020.05.015
70. Mbala GFO, Mveme CDD, Ntieche Z, Ejuh GW, Ndjaka JMB, Abe MTO (2021) Effect of chlorine and bromine on the nonlinear optical, electronic, optoelectronic and thermodynamic properties on the BEDT-TTF molecule: ab-initio and DFT calculations. Opt Quantum Electron 576. https://doi.org/10.1007/s11082-021-03211-4
71. de Andrade AM, Inacio PL, Camilo A Jr (2015) Theoretical investigation of second hyperpolarizability of trans-polyacetylene: comparison between experimental and theoretical results for small oligomers. J Chem Phys 244906. https://doi.org/10.1063/1.4939083
72. Veillard A (1970) Relaxation during internal rotation ethane and hydrogen peroxyde. Theor Chim Acta 21–33. https://doi.org/10.1007/BF00533694
73. M Cardona et al. R Merlin (2007) Light scattering in solids IX. In: Cardona M, Merlin R (ed) Topics in applied physics, Springer Berlin, Heidelberg, pp 1–14. https://doi.org/10.1007/978-3-540-34436-0_1
74. Colthup NB, Daly LH, Wiberley SE (1990) Chapter 1 - Vibrational and rotational spectra. In: Colthup NB, Daly LH, Wiberley SE (ed) Introduction to Infrared and Raman Spectroscopy, 3rd edn. Academic Press, San Diego, pp 1–73. https://doi.org/10.1016/B978-0-08-091740-5.50004-1
75. Prinsloo LC, du Plooy W, van der Merwe C (2004) Raman spectroscopic study of the epicuticular wax layer of mature mango (Mangifera indica) fruit. J Raman Spectrosc 561–567. https://doi.org/10.1002/jrs.1185
76. Baldenebro-López J, Castorena-González J, Flores-Holguín N, Almaral-Sánchez J, Glossman-Mitnik D (2012) Density Functional Theory (DFT) Study of Triphenylamine-Based Dyes for Their Use as Sensitizers in Molecular Photovoltaics. Int J Mol Sci Art n° 4. https://doi.org/10.3390/ijms13044418
77. Krishnakumar V, Xavier RJ (2023) Normal coordinate analysis of 2-mercapto and 4,6-dihydroxy -2-mercapto pyrimidines, IJPAP. http://nopr.niscpr.res.in/handle/123456789/25217
78. Gunasekaran S, Seshadri S, Muthu S, Kumaresan S, Arunbalaji R (2008) Vibrational spectroscopy investigation using ab initio and density functional theory on p-anisaldehyde. Spectrochim Acta A Mol Biomol Spectrosc 550–556. https://doi.org/10.1016/j.saa.2007.07.050
79. Kumru M, Küçük V, Kocademir M (2012) Determination of structural and vibrational properties of 6-quinolinecarboxaldehyde using FT-IR, FT-Raman and Dispersive-Raman experimental techniques and theoretical HF and DFT (B3LYP) methods. Spectrochim Acta A Mol Biomol Spectrosc 242–251. https://doi.org/10.1016/j.saa.2012.05.001
80. Tadjouteu Assatse Y, Ejuh GW, Tchoffo F, Ndjaka JMB (2019) DFT studies of nanomaterials designed by the functionalization of modified carboxylated carbon nanotubes with biguanide derivatives for nanomedical, nonlinear and electronic applications. Chin J Phys 253–262. https://doi.org/10.1016/j.cjph.2019.01.014
81. Barnes AJ, Majid MA, Stuckey MA, Gregory P, Stead CV (1985) The resonance Raman spectra of Orange II and Para Red: molecular structure and vibrational assignment. Spectrochim Acta Part Mol Spectrosc 629–635. https://doi.org/10.1016/0584-8539(85)80050-7
82. Socrates G (2004) Infrared and Raman characteristic group frequencies: tables and charts. John Wiley & Sons
83. Jacox ME (2003) Vibrational and electronic energy levels of polyatomic transient molecules. Supplement B. J Phys Chem Ref Data 1–441. https://doi.org/10.1063/1.1497629
84. GW Ejuh, F Tchangnwa Nya, MT Ottou Abe, FF Jean-Baptiste, et al. JMB Ndjaka (2017) Electronic structure, physicochemical, linear and non linear optical properties analysis of coronene, 6B-, 6N-, 3B3N- substituted C24H12 using RHF,

B3LYP and wB97XD methods », Opt. Quantum Electron., 382 https://doi.org/10.1007/s11082-017-1221-2
85. CDD Mveme, F Tchangnwa Nya, GW Ejuh, et al. JMB Ndjaka (2021) A density functional theory (DFT) study of the doping effect on 4-[2-(2-N, N-dihydroxy amino thiophene) vinyl] benzenamine, SN Appl Sci, 317
86. Bosshard Ch, Bösch M, Liakatas I, Jäger M, Günter P (2000) Second-order nonlinear optical organic materials: recent developments. In: Günter P (ed) Nonlinear optical effects and materials, Springer Series in Optical Sciences, Berlin, Heidelberg: Springer, pp 163–299. https://doi.org/10.1007/978-3-540-49713-4_3
87. Usman Khan M et al (2023) DFT molecular simulations for static, dynamic and solvent-dependent nonlinear optical properties of triphenylamine-carbazole-based organic dyes with D-D-A framework. J Molecular Liquids 12325. https://doi.org/10.1016/j.molliq.2023.123258
88. K Fukui (1982) Role of Frontier Orbitals in Chemical Reactions, Science, (747-754) https://doi.org/10.1126/science.218.4574.747
89. MU Khan et al. (2024) Theoretical study of static and frequency-dependent nonlinear optical properties of 1-phenyl-2,5-di(thiophen-2-yl)-1H-pyrrole based D-π-A chromophores through π-linkers modifications: A gateway towards giant nonlinear optical compounds, Materials Sci Eng: B, 116993
90. Parr RG, Pearson RG (n.d.) Absolute hardness: companion parameter to absolute electronegativity. ACS Publications. https://pubs.acs.org/doi/pdf/10.1021/ja00364a005
91. C Andraud et al. (n.d.) Theoretical and experimental investigations of the nonlinear optical properties of vanillin, polyenovanillin, and bisvanillin derivatives, ACS Publications
92. Geskin VM, Lambert C, Brédas J-L (2003) Origin of high second- and third-order nonlinear optical response in ammonio/borato diphenylpolyene zwitterions: the remarkable role of polarized aromatic groups. J Am Chem Soc 15651–15658. https://doi.org/10.1021/ja035862p
93. Nakano M, Fujita H, Takahata M, Yamaguchi K (2002) Theoretical study on second hyperpolarizabilities of phenylacetylene dendrimer: toward an understanding of structure−property relation in NLO responses of fractal antenna dendrimers. J Am Chem Soc 9648–9655. https://doi.org/10.1021/ja0115969
94. Kolinsky PV (1992) New materials and their characterization for photonic device applications. Opt Eng 1676–1684. https://doi.org/10.1117/12.58844
95. Eaton DF (1991) Nonlinear optical materials. Science 281–287. https://doi.org/10.1126/science.253.5017.281
96. Y-X Sun et al. (2009) Experimental and density functional studies on 4-(3,4-dihydroxybenzylideneamino)antipyrine, and 4-(2,3,4-trihydroxybenzylideneamino)antipyrine, J Mol Struct THEOCHEM, (74-82)
97. Saji RS, Prasana JC, Muthu S, George J, Kuruvilla TK, Raajaraman BR (2020) Spectroscopic and quantum computational study on naproxen sodium. Spectrochim Acta A Mol Biomol Spectrosc 117614. https://doi.org/10.1016/j.saa.2019.117614
98. Kaatz P, Donley EA, Shelton DP (1998) A comparison of molecular hyperpolarizabilities from gas and liquid phase measurements. J Chem Phys 849–856. https://doi.org/10.1063/1.475448
99. Hendrickx E, Clays K, Persoons A (1998) Hyper-Rayleigh scattering in isotropic solution. Acc Chem Res 675–683. https://doi.org/10.1021/ar960233o
100. Ohnoutek L et al (2020) Single nanoparticle chiroptics in a liquid: optical activity in Hyper-Rayleigh scattering from Au helicoids. Nano Lett 5792–5798. https://doi.org/10.1021/acs.nanolett.0c01659
101. Castet F, Bogdan E, Plaquet A, Ducasse L, Champagne B, Rodriguez V (2012) Reference molecules for nonlinear optics: a joint experimental and theoretical investigation. J Chem Phys 024506. https://doi.org/10.1063/1.3675848
102. Bree C, Demircan A, Steinmeyer G (2010) Method for computing the nonlinear refractive index via Keldysh theory. IEEE J Quantum Electron 433–437. https://doi.org/10.1109/JQE.2009.2031599
103. Milam D (1998) Review and assessment of measured values of the nonlinear refractive-index coefficient of fused silica. Appl Opt 546–550. https://doi.org/10.1364/AO.37.000546
104. M Sheik-Bahae, AA Said, T-H Wei, DJ Hagan, et al. EW Van Stryland (1990) Sensitive measurement of optical nonlinearities using a single beam, IEEE J Quantum Electron, (760-769)
105. Landolt B (1978) Numerical data and functional relationships in science and technology. Magn Another Prop Oxides Relat Compd Pt Garnets Perovscites. https://cir.nii.ac.jp/crid/1572824499577656064
106. Gubler U, Bosshard C (2000) Optical third-harmonic generation of fused silica in gas atmosphere: absolute value of the third-order nonlinear optical susceptibility. Phys Rev B 10702–10710. https://doi.org/10.1103/PhysRevB.61.10702
107. Dai L (1999) Advanced syntheses and microfabrications of conjugated polymers, C60-containing polymers and carbon nanotubes for optoelectronic applications. Polym Adv Technol 357–420. https://doi.org/10.1002/(SICI)1099-1581(199907)10:7<357::AID-PAT886>3.0.CO;2-9
108. Hirata S, Head-Gordon M, Szczepanski J, Vala M (2003) Time-dependent density functional study of the electronic excited states of polycyclic aromatic hydrocarbon radical ions. J Phys Chem A 4940–4951. https://doi.org/10.1021/jp0301913
109. Shen Y et al (2016) Deep-ultraviolet transparent Cs2LiPO4 exhibits an unprecedented second harmonic generation. Chem Mater 7110–7116. https://doi.org/10.1021/acs.chemmater.6b03333

Authors and Affiliations

C. D. Ribouem A. Bessong[1] · M. T. Ottou Abe[1] · Zounedou Ntieche[1,2] · P. Noudem[1] · J. B. Fankam Fankam[3] · J. M. B. Ndjaka[1]

✉ C. D. Ribouem A. Bessong
charlesdouglas95@yahoo.fr

✉ M. T. Ottou Abe
ottouthierry85@yahoo.fr

[1] Faculty of Science, Department of Physics, University of Yaoundé I, P.M.B 812, Yaoundé, Cameroon

[2] Local Material Promotion Authority (MIPROMALO), P.O. Box 2396, Yaoundé, Cameroon

[3] Molecular Sciences Institute, School of Chemistry, University of the Witwatersrand, Johannesburg 2050, South Africa